ON THE VERGE OF BIOORGANIC AND INORGANIC CHEMISTRY: METALLACARBORANES IN NANOMEDICINE

Adnana Alina Zaulet

TESI DOCTORAL

Programa de Doctorat en Química

Director: Prof. Clara Viñas i Teixidor

Tutor: Josefina Pons Picart

Departament de Química

Facultat de Ciències

2015

OBJECTIVES

OBJECTIVES

The main objective of this PhD thesis was the synthesis of anionic $[M(C_2B_9H_{11})_2]^-$ metallabis(dicarbollide) derivatives, for their potential use as molecular materials and biomaterials in a wide variety of applications.

The objective to apply anionic halogenated metallabis(dicarbollide) derivatives in molecular materials was based on the chemical composition of the metallabis(dicarbollide) framework: i) the presence of the metal, Co or Fe, η^5 bonded to two $[C_2B_9H_{11}]^{2-}$ ligands that can go under a redox process and ii) the possibility of the hydrogen substitution at the B-H vertices to produce B-Me and B-X (X= I, Cl) bonds. The influence of the methyl groups as well as the halogen atoms (I and Cl) bonded to the boron vertices of the cluster on the electrochemical properties of the sandwiched metal needed to be studied. To achieve this objective, the synthesis, isolation and characterization of large families of compounds has been firstly required. Then, electrochemical studies of all species would be run. Based on their $E_{1/2}$ potential, selected compounds would be tested as electrolytes in the DSSC devices.

The application of the anionic halogenated metallabis(dicarbollide) derivatives in biomaterials was based on: i) the anionic nature of the $[M(C_2B_9H_{11})_2]^-$ metallabis(dicarbollide) (M= Co and Fe) framework that provides water solubility and ii) the possibility to carry out poly- hetero- substitutions at the *exo*-cluster hydrogen atoms of the cluster. For biomedical application, the physic-chemical properties of biocompatible salts of pristine anionic $[M(C_2B_9H_{11})_2]^-$ needed to be carefully studied. Next, the possibility to obtain multifunctional $[M(C_2B_9H_{11})_2]^-$ compounds needed to be investigated. To achieve this objective, disubstituted hetero metallabis(dicarbollide) derivatives containing an iodine atom and a PEG branch ended with a biomolecule needed to be synthesized, isolated and characterized. Then, radio imaging studies *"in vivo"* would be required.

RESULTS AND DISCUSSIONS

2.1- Methylated and halogenated metallabis(dicarbollide) derivatives

2.1.1.- Methylated anionic cobaltabis(dicarbollide) derivatives

From the previous thesis in our group[1], we knew that the incorporation of iodine atoms and methyl groups bonded *exo*-cluster to boron vertexes of the neutral *o*-carborane framework causes a significant electronic effect on $^{11}B\{^1H\}$ NMR chemical shift of the boron atom to which the substituent is bonded, as well modifying the acidic character of the H atoms of the C_c-H vertexes. In the case of *o*-carborane derivatives, the electron withdrawing or donating character of the substituent (Me or I) was proved by NMR spectroscopy and supported by theoretical calculations.[2] Methyl groups, when attached to boron, are electron-withdrawing;[2] whereas iodine atoms bonded to boron act as electron donors, probably via π-donation. In addition, the incorporation of iodine atoms onto the boron vertexes of the *o*-carborane framework causes a uniform increase in the acidic character of the C_c-H, whereas the presence of methyl groups reduces their acidity.[2]

In order to study the electronic effect of the methyl groups on the redox potential of the couple Co^{3+}/Co^{2+} of the anionic cobaltabis(dicarbollide), the synthesis and isolation of several methylated cobaltabis(dicarbollide) species were carried out. In 1996, Hawthorne and co [3] reported the hexamethylated derivative of cobaltabis(dicarbollide) that was obtained by a modification of Kumada reaction. The incorporation of one and two methyl groups bonded *exo*-cluster to boron vertexes of the anionic cobaltabis(dicarbollide) was done later, by our group.[4]

To complete this part of research, two new methylated derivatives have been synthesized in this thesis: the tetramethylated derivative, $[Me_4\text{-}\mathbf{3}]^-$, and octamethylated derivative, $[Me_8\text{-}\mathbf{3}]^-$. The $[Me_4\text{-}\mathbf{3}]^-$ was produced by a Kumada cross-coupling reaction on tetraiodinated derivative, in the presence of $[PdCl_2(PPh_3)_2]$ and CuI as catalysts and the Grignard reagent as the source of methyl groups (Scheme 2.1).

The complex $[Me_4\text{-}\mathbf{3}]^-$ is an anionic cluster so one the most efficient method for characterization is the ionization technique: Matrix-Assisted Laser Desorption/Ionization (MALDI-TOF-MS).

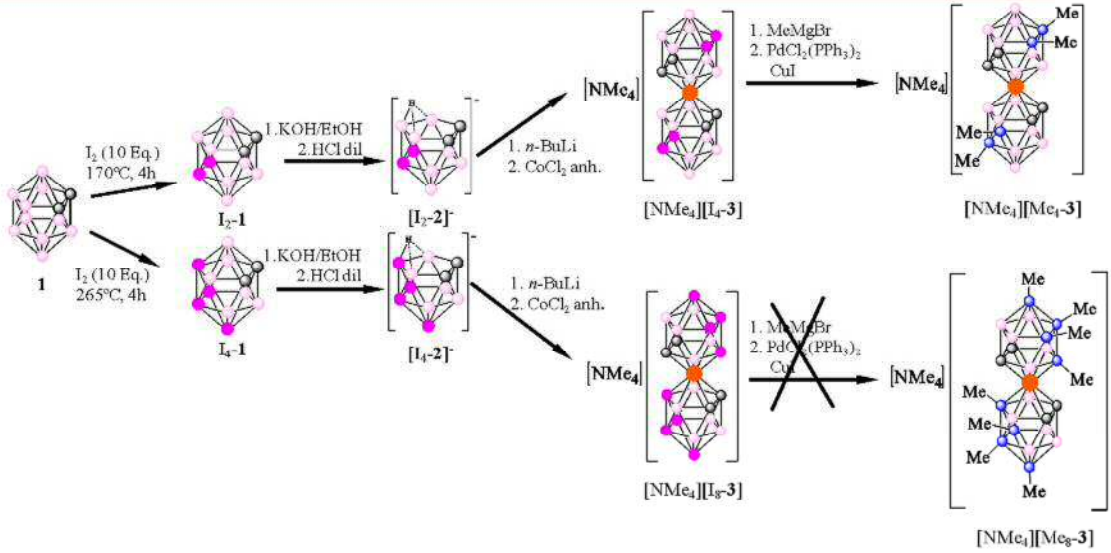

Scheme 2.1. General scheme for the synthesis of $[NMe_4][Me_4\text{-}3]$.

In the Figure 2.1 is illustrated the molecular peak at m/z 379 cm^{-1} with a separation between isotopic peaks distribution of **1**, that correspond to the tetramethylated species. The $^{11}B\{^1H\}$-NMR of the tetramethylated complex (Figure 2.2) contains the same numbers of resonances (five) as the parent tetraiodo cobaltabis(dicarbollide) $[I_4\text{-}3]^-$ but a different pattern: 1:1:2:4:1 for $[I_4\text{-}3]^-$ and 1:3:2:2:1 for $[Me_4\text{-}3]^-$. The resonance at +4.08 ppm exhibits no splitting in the proton coupled boron NMR spectrum and was assigned as the resonance of the four B-Me vertexes. To notice that the substitution of iodine with methyl group cause a significant deshielding on boron atoms attached to the substituent. $^{11}B\{^1H\}$-NMR showed that a methyl group bonded *exo*-cluster to a boron vertex of the anionic cobaltabis(dicarbollide) cluster is electron

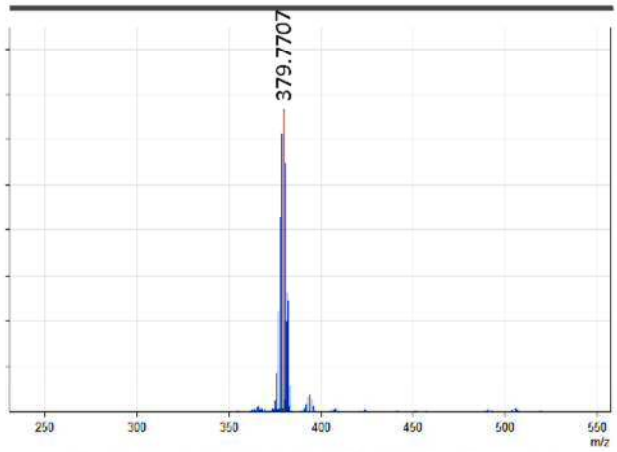

Figure 2.1. MALDI-TOF-MS of complex $[Me_4\text{-}3]^-$.

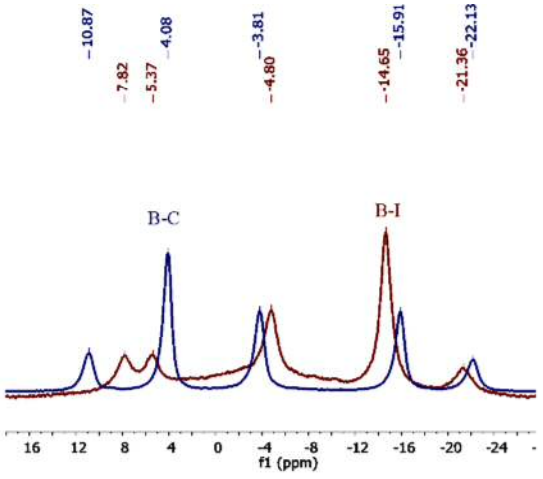

Figure 2.2. $^{11}B\{^1H\}$-NMR comparison between $[Me_4\text{-}3]^-$ (blue) and $[I_4\text{-}3]^-$ (red).

withdrawing, in the same way as in the neutral *o*-carborane. Crystals of [Me_4-**3**]$^-$ suitable for X-ray diffraction were obtained by slow evaporation of a dichloromethane/chlorofom solution. As it is showed in Figure 2.3, the structure was found in a *cisoid* conformation. The bond lengths B-Me are B(9)-C(9) = 1.611Å, B(12)-C(12) = 1.594Å, B(9')-C(9') = 1.592Å, B(12')-C(12') = 1.583Å. These distances are shorter than, for ex. in [Me_6-**3**]$^-$ where the shortest B(12)-Me bond length is 1.63Å.3

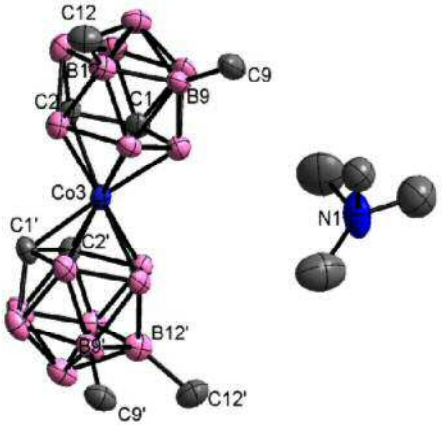

Figure 2.3. Crystal structure of [NMe_4][Me_4-**3**].

We tried out the same reaction conditions in order to obtain the octamethylated derivative [Me_8-**3**]$^-$, but we were not successful. An uncontrolled mixture of compounds was obtained. For this reason, we changed the synthesis strategy (Scheme 2.2).

Starting from tetramethyl *o*-carborane, we attempted to the partial deboronation reaction of the *closo* species, using as nucleophile the potassium etoxide. The NMR spectrum of the crude of the reaction indicated that after overnight reflux and 10 eq. of KOH, there was still a large amount of the starting closo Me_4-**1**. So, deboronation using potassium hydroxide/ethanol has its limitations. Although other deboronation reagents such as tertiary amines, hydrazine, ammonia, piperidine and pyrrolidine are also available, the fluoride ion was a promising alternative because it is a very weak nucleophile but effective as well easy to handle.[5] The system CsF (5 eq.) / ethanol and 2 days of reflux was not efficient in order to obtain the *nido* species. By increasing the number of equivalent of CsF from 5 to 20, the ^{11}B-NMR spectrum of the reaction crude, showed the appearance of the *nido* peaks but not the total conversion of the *closo* into the corresponding *nido* cluster.

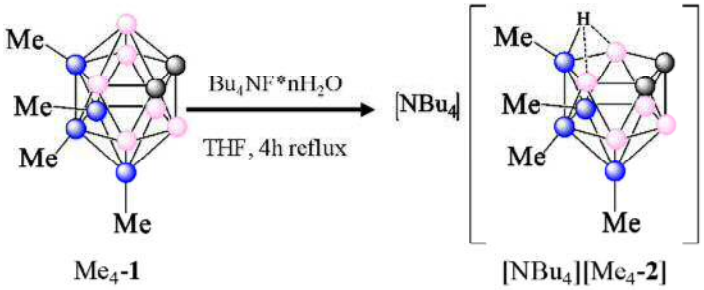

Scheme 2.2. Partial deboronation of *closo* Me_4-**1**.

Wade *et al.* reported[5b] that hydrated tetrabuthylammonium fluoride in THF is a good reagent for deboronation of *closo*-*o*-carborane and their aryl derivatives to the

corresponding *nido* species. The experiments were carried out all of them with the hydrate form of tetrabuthylammonium fluoride and it was found out that water plays an important role in the deboronation reaction. It was observed that the speed of the reaction was increased by addition of small amounts of water.

We attempt partial deboronation of *closo* Me_4-**1** to *nido* $[Me_4\text{-}\mathbf{2}]^-$ using hydrated tetrabuthylammonium floride in a ratio F^- : Me_4-**1** (5:1).

The partial deboronation reaction was monitored by ATR and as it is showed in

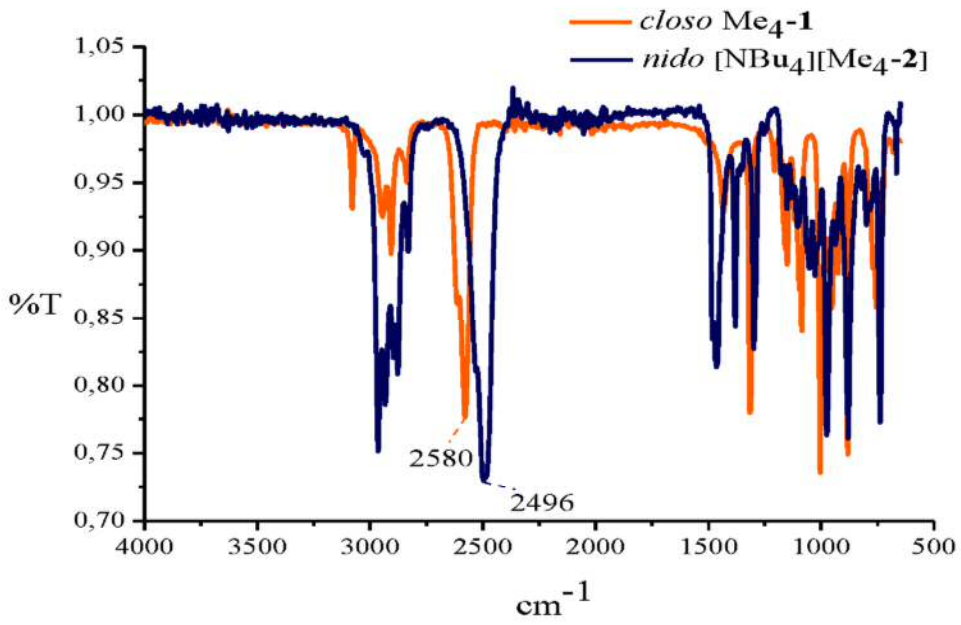

Figure 2.4. Comparison of ATR spectra between *closo* Me_4-**1** (orange) and *nido* $[NBu_4][Me_4\text{-}\mathbf{2}]$ (blue).

the Figure 2.4, it was considered to be completed when the B-H band at 2580 cm^{-1} that belongs to the *closo* Me_4-**1,** had completely disappeared and it was replaced by the frequency at 2496 cm^{-1} that corresponds to the *nido* $[Me_4\text{-}\mathbf{2}]^-$. After 4 h refluxing, the compound $[Me_4\text{-}\mathbf{2}]^-$ was extracted in dicholomethane and the resulting oil was washed with hexane to give 92% yield of $[Me_4\text{-}\mathbf{2}]^-$ as a white solid.

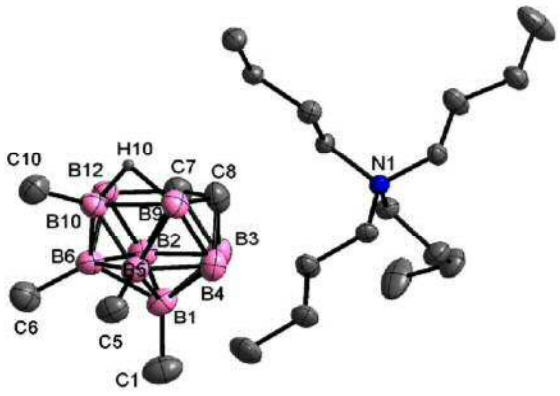

Figure 2.5. Crystal structure of $[NBu_4][Me_4\text{-}\mathbf{2}]$.

Once we established the procedure for the synthesis of *nido* $[Me_4\text{-}\mathbf{2}]^-$, we performed also the degradation of *closo* compound, Me_2-**1**. The partial degradation of

Me_2-**1** to the *nido* [Me_2-**2**]$^-$ was accomplished in 20 h of reflux using 5 Eq. of potassium etoxide. It has been characterized by spectroscopic and spectrometric techniques such as ^{1}H-NMR, ^{11}B-NMR, ^{13}C-NMR and MALDI-TOF-MS that confirmed the synthesis of the desired compound. Crystals of [NBu_4][Me_4-**2**], suitable for X-ray diffraction were grown from ethanol (illustrated in Figure 2.5). The B-C distances were determined to be 1.579(4) (B6-C6), 1.592(4) (B3-C3), 1.593(5) (B1-C1), 1.619(4) (B4-C4), which lie within the range of distances known for methylated borane clusters.[3,4]

The Table 2.1 displays the characterization by ^{1}H{^{11}B}-NMR of the *closo* methylated and the corresponded *nido* species.

Compound	δ (C_c-H)	δ (B-Me)	δ (B-H)	δ (H_{bridge})
closo Me_2-**1**	4.26	0.17	2.73, 2.50, 1.76, 1.28	-
nido [Me_2-**2**]$^-$	1.53	-0.04	1.96, 1.29, 0.37, 0.19	-2.48
closo Me_4-**1**	4.14	0.18, -0.03	2.80, 1.86	-
nido[Me_4-**2**]$^-$	-	0.05, -0.29	1.72, 1.12	-1.88

Table 2.1. ^{1}H{^{11}B}-NMR chemical shift of the *closo*: Me_2-**1**, Me_4-**1** and *nido* compounds: [Me_2-**2**]$^-$, [Me_4-**2**]$^-$.

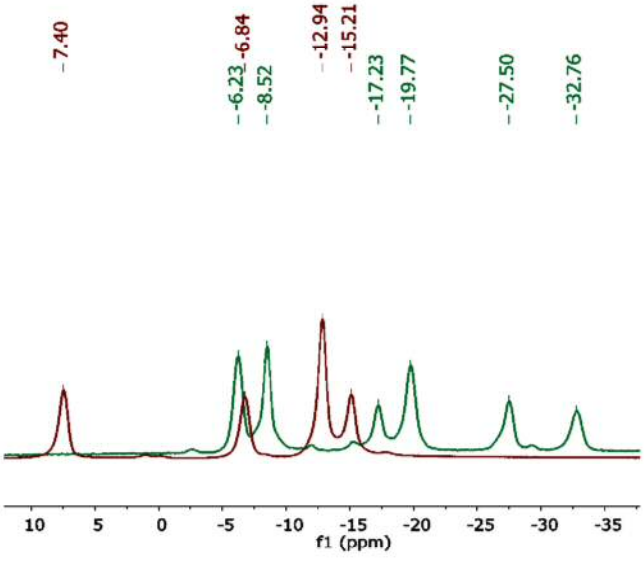

Figure 2.6. ^{11}B{^{1}H}-NMR comparison between Me_2-**1** (red) and [Me_2-**2**]$^-$ (green).

Figure 2.6 presents the ^{11}B{^{1}H}-NMR spectra before (red) and after (green) the partial deboronation of compound *closo* Me_2-**1**. The pattern and chemical shift range of the ^{11}B-NMR spectra showing two peaks at high field, -33 and -27 ppm are a clear indication that the deboronation reaction was completed.

These *nido* anionic ligands are the precursors of the methylated metallacarboranes. To obtained the sandwich cobaltabis(dicarbollide), the *nido* [Me_4-**2**]$^-$ compound was treated with K^{t}BuO in anhydrous THF to remove the H bridge and produce the dicarbollide dianion in solution. Reaction of the latter with anhydrous $CoCl_2$ led to the formation of [Me_8-**3**]$^-$

complex (Scheme 2.3). The anions were isolated as salt of tetramethyl ammonium. The two methylated complexes, $[Me_8\text{-}\mathbf{3}]^-$ and $[Me_4\text{-}\mathbf{3}]$, were characterized by conventional techniques. The IR spectra confirm the formation of the complex $[Me_8\text{-}\mathbf{3}]^-$ because the absorption band of the B-H at 2496 cm^{-1} that corresponds to the *nido*, moves to 2557 cm^{-1}. The ^{1}H-NMR spectrum of $[Me_8\text{-}\mathbf{3}]^-$ displays in addition to the signals for the tetrabuthylammonium counterion, resonances for the C_c-H vertexes at 4 ppm and the ones that correspond to the eight B-Me at 0.09, 0.05 and -0.19 ppm and broad signals corresponding to B-H bonds.

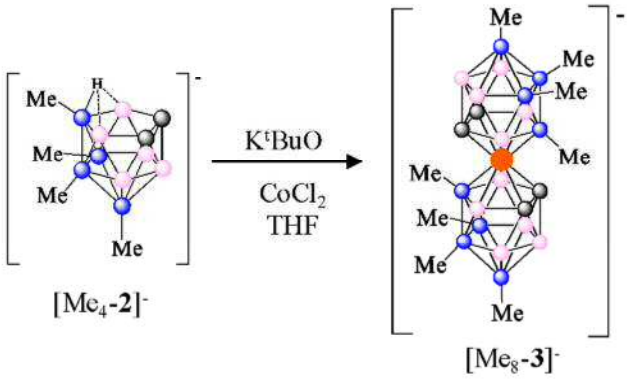

Scheme 2.3. Complexation reaction of *nido*, $[Me_4\text{-}\mathbf{2}]^-$.

2.1.2.- Halogenated anionic cobaltabis(dicarbollide) derivatives

2.1.2.a.- Iodinated derivatives

Highly iodinated molecules have been of interest in materials science and medical applications including the potential use of iodinated *ortho*-carboranes as next generation radiopaque contrast agents for X-ray diagnosting imaging.[6]

Previously in our group[7] the *closo* 8,9,10,12-I_4-$C_2B_{10}H_8$, I_4-**1**, had been tested as X-ray contrast in bone cements due to its high iodine content (78.4%), exceptional stability and its complete insolubility in aqueous media. The experiments showed a good cell-compatibility *in vitro* as well as a sufficient radiopacity.

The first example of direct halogen substitution in metallacarborane was done by Hawthorne et *al.* in 1967 to obtain brominated species of $[3,3'\text{-Co-}(1,2\text{-}C_2B_9H_{11})_2]^-$.[8]

There are 2 ways for the synthesis of substituted metallacarborane: 1) the direct substitution route on cobaltabis(dicarbollide) cluter; 2) the synthesis of iodinated cobaltabis(dicarbollide) starting from *closo* iodinated *o*-carborane ligands followed by their degradation to the corresponding *nido* ligands and finally their complexation with metal such Co or Fe.

1) The direct route iodination substitution of the B-H vertices of the cobaltabis(dicarbollide), $[\mathbf{3}]^-$ framework by B-I.

Taking into account the hydride character of hydrogen atoms bonded to boron, the incorporation of iodine atoms involve an Electrofile Induced Nucleophilic Substitution (EINS) reaction. The mechanism include the attack of the electrophilic agent, followed by the elimination reaction of the hydrogen atom as a hydride to form a pseudoelectrofilic centre on the boron atom which is susceptible to a nucleophilic attack. So, mono $[\text{I-}\mathbf{3}]^-$,[4a] di $[\text{I}_2\text{-}\mathbf{3}]^-$ [4b] and hexaiodinated $[\text{I}_6\text{-}\mathbf{3}]^-$ [3] derivatives have been obtained following this reaction in high yield.

2) The indirect route of $[\mathbf{3}]^-$ iodinated derivatives.

o-Carborane can be regioselective di and tetraiodinated using a solvent free reaction method. The electrophilic diiodination at the 9 and 12 position, and tetraiodination at the 8,9,10 and 12 vertexes by treatment with iodine in a ratio 1:10 in sealed tubes under different experimental conditions (temperature and reaction times) opens the possibility on synthesis or on incorporate new molecules. The partial deboronation step of the previously *closo* species to the corresponding *nido* compounds $[\text{I}_2\text{-}\mathbf{2}]^-$, $[\text{I}_4\text{-}\mathbf{2}]^-$ followed by the complexation with $CoCl_2$ give rise to the tetra and octaiodinated derivatives of cobaltabis(dicarbollide), $[\text{I}_4\text{-}\mathbf{3}]^-$, $[\text{I}_8\text{-}\mathbf{3}]^-$ that were isolated by precipitation as tetramethylammonium salts.

i) Calcium salts

Knowing that the chemical composition of the bones is around 45% minerals (calcium carbonates and fosfates), we had in mind the possible application of such highly iodinated anionic compounds as radiopaque agents in vertebloplasty.

To achieve it, the $[NMe_4]^+$ cation of $[\text{I}_4\text{-}\mathbf{3}]^-$ and $[\text{I}_8\text{-}\mathbf{3}]^-$ was changed by calcium using anionic exchange resin. After the preparation, these two compounds, $Ca[\text{I}_4\text{-}\mathbf{3}]_2$ and $Ca[\text{I}_8\text{-}\mathbf{3}]_2$ were characterized employing spectroscopic and spectrometric techniques such as ATR, MALDI-TOF-MS, ^{1}H, ^{11}B-NMR and also Scanning Electron Microscopy. Thermal techniques as Thermogravimetric analysis (TGA) and Differential Scanning Calorimetry (DSC) gave information about the number of coordination water molecules to calcium cation.

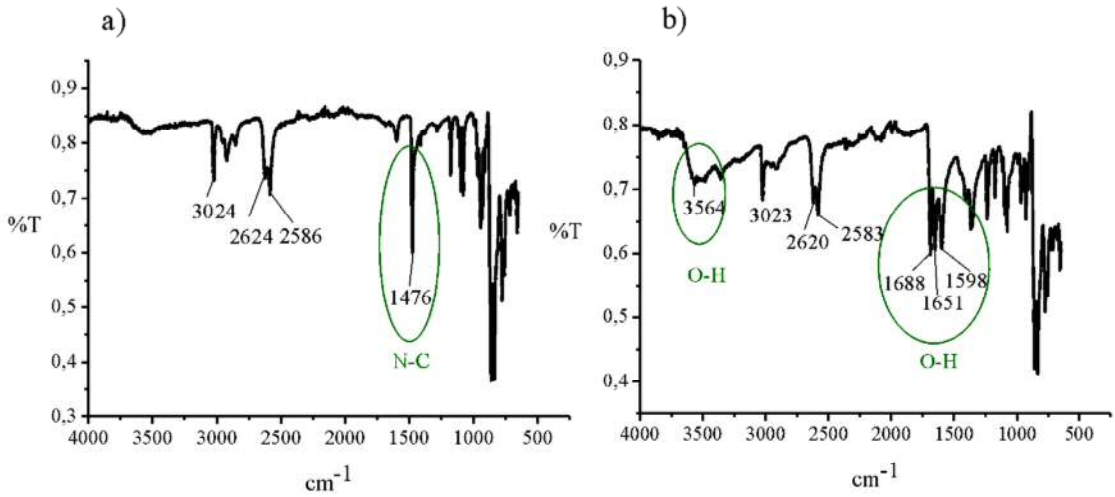

Figure 2.7. Comparison between the IR spectra of a) $[NMe_4][I_8\text{-}\mathbf{3}]$ and b) $Ca[I_8\text{-}\mathbf{3}]_2$.

The comparison between the infrared spectra of the starting compound $[NMe_4][I_8\text{-}\mathbf{3}]$ and the $Ca[I_8\text{-}\mathbf{3}]_2$ salt confirmed the interchanging of the tetramethyl cation by calcium: the absorption band of the N-C bond (1476 cm^{-1}) disappeared in the final compound. It is also interesting to observe that the IR spectrum of the calcium compound (Figure 2.7, right) displays absorption bands at 3564 cm^{-1}, 1688 cm^{-1}, 1651 cm^{-1} and 1598 cm^{-1} that correspond to H_2O.

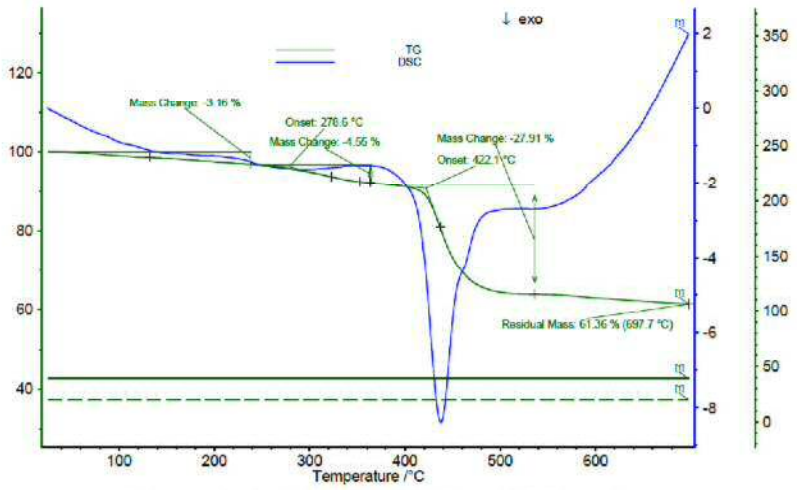

Figure 2.8. TGA and DSC of $Ca[I_8\text{-}\mathbf{3}]_2$.

Thermal analysis, TGA and DSC (Figure 2.8), confirm the presence of H_2O molecules coordinates Ca^{2+} in the compounds. The TGA is a technique that gives quantitative data on the loose of mass of a solid when the temperature is increasing. So, we observed a loose of mass until 270 °C that correspond to 5 molecules of H_2O and a weight loss of 27.91%, at 420°C attributable to the loss of 6 iodine atoms.

Another technique that was very useful for us and could prove the presence of Calcium in the two compounds was scanning electron microscope (SEM). SEM is a characterization technique for materials that offer information about the morphology (texture) and chemical composition, some of them at the nanometric scale.

From Figure 2.9, is clearly observed the presence of calcium, iodine, boron, carbon, oxygen and cobalt.

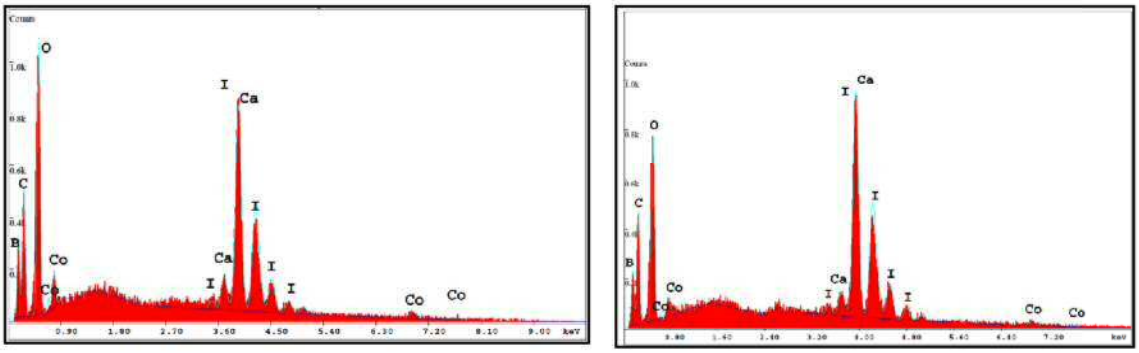

Figure 2.9. Chemical composition of $Ca[I_4\text{-}\mathbf{3}]_2$ (left) and $Ca[I_8\text{-}\mathbf{3}]_2$ (right).

Figures 2.10 and 2.11 display the morphology of $Ca[I_8\text{-}\mathbf{3}]_2$ and $Ca[I_4\text{-}\mathbf{3}]_2$ with magnification sections.

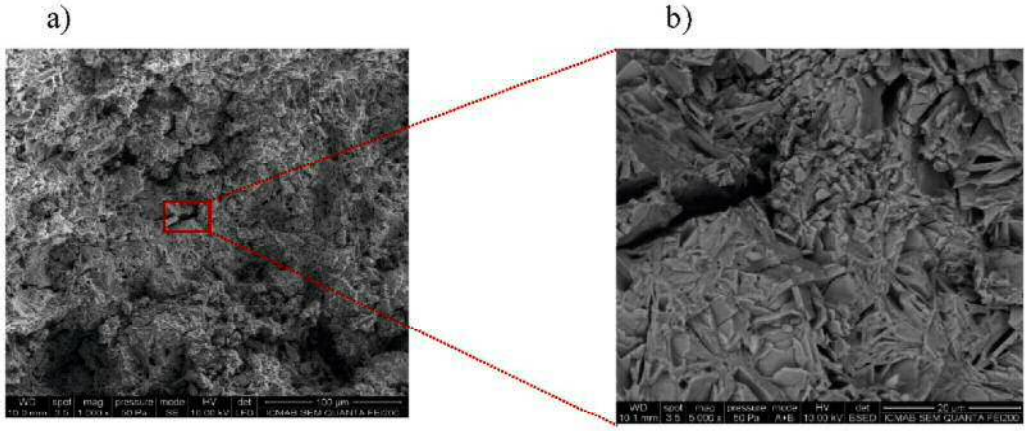

Figure 2.10. a) SEM images for $Ca[I_8\text{-}\mathbf{3}]_2$; scale bar 100 μm.
b) magnification section; scale bar 20 μm.

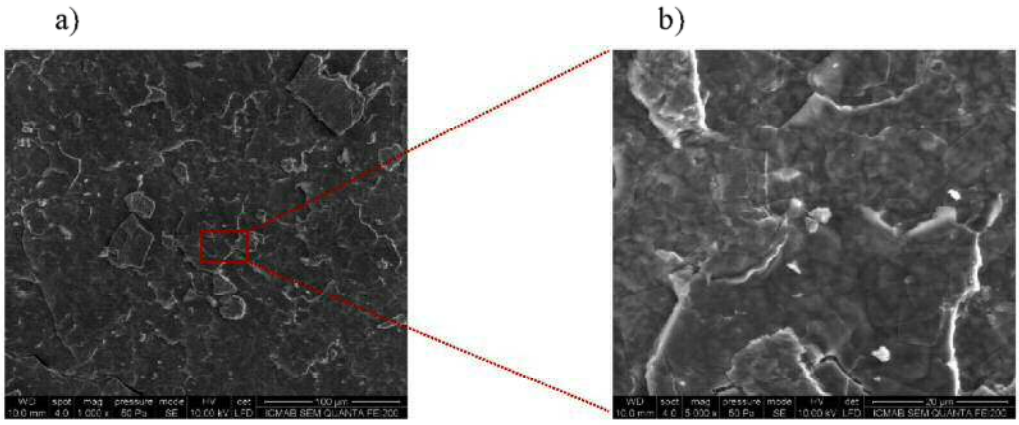

Figure 2.11. a) SEM images for $Ca[I_4\text{-}\mathbf{3}]_2$; scale bar 100 μm.
b) magnification; scale bar 20 μm.

Because SEM is capable of performing analysis of selected point locations on the sample, it can be useful in qualitatively or semi-quantitatively determination of chemical compositions. In Table 2.2 we can see the percentage of calcium in the two samples, 2.45% for the tetraiodinated derivative and 1.95% for the octaiodinated specie,

$Ca[I_4\text{-}\mathbf{3}]_2$				$Ca[I_8\text{-}\mathbf{3}]_2$			
Element	Calculated	Wt%	At%	Element	Calculated	Wt%	At%
B	22.96	19.82	52.06	**B**	14.40	14.50	46.84
C	5.67	8.50	20.10	**C**	3.56	7.35	21.36
O		5.53	9.81	**O**		3.94	8.60
Ca	2.36	2.45	1.74	**Ca**	1.48	1.95	1.70
I	59.90	55.84	12.50	**I**	75.15	67.17	18.48
Co	6.95	7.86	3.79	**Co**	4.36	5.08	3.01

Table 2.2. Percentage of different elements.

but we can't affirm that is the real amount of calcium in the sample. For this, it is recommended to use other techniques.

The ^{1}H-NMR and $^{13}C\{^1H\}$-NMR spectra (Table 2.3) of $Ca[I_4\text{-}\mathbf{3}]_2$ and $Ca[I_8\text{-}\mathbf{3}]_2$ were run in d^6-acetone. The ^{1}H-NMR spectra display the resonance of the coordinated H_2O at 3.38 and 3.33 ppm, respectively. ^{1}H-NMR spectrum of $Ca[I_8\text{-}\mathbf{3}]_2$, (Figure 2.12), provide information on the number of coordinated H_2O: 2.5 molecules of H_2O per molecule of $Ca[I_8\text{-}\mathbf{3}]_2$. There is practically no difference between the chemical shift of the ^{1}H and $^{13}C\{^1H\}$ of the vertex C_c-H in the two salts, $[NMe_4]^+$ and Ca^{2+}.

Entry	δ (^{1}H) ppm			δ (^{13}C) ppm	
	C_c-H	H_2O	NMe_4	C_c-H	NMe_4
$[NMe_4][I_4$-**3**$]$	4.46		3.47	49.11	55.29
$Ca[I_4$-**3**$]_2$	4.46	3.38	-	49.09	-
$[NMe_4][I_8$-**3**$]$	5.14		3.47	60.78	55.32
$Ca[I_8$-**3**$]_2$	5.14	3.33	-	60.78	-

Table 2.3. ^{1}H-NMR and ^{13}C-NMR signals for the two different salt of tetra and octa iodinated cobaltabis(dicarbollide).

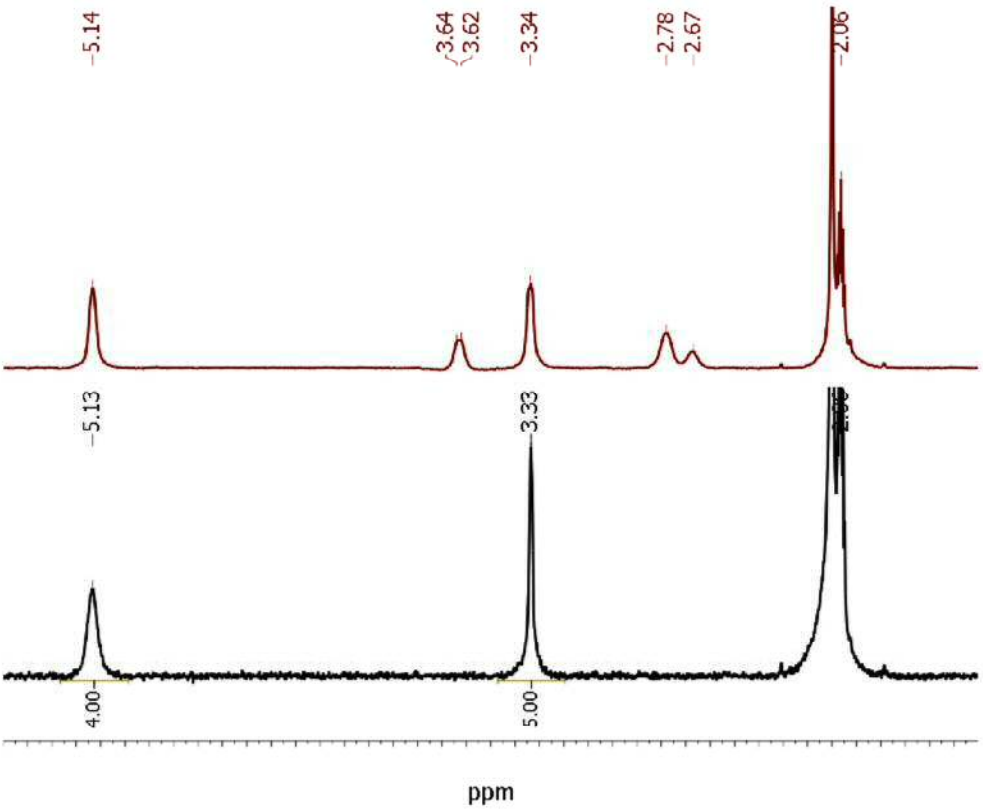

Figure 2.12. Comparison between ^{1}H-NMR and ^{1}H{^{11}B}-NMR for $Ca[I_8$-**3**$]_2$.

ii) Silver salts

The sandwich complexes such cobaltabis(dicarbollide) can be used as very weakly coordinating anions and may coordinate to Ag (I) through B-H···Ag interactions and the halogenated derivatives coordinate to metal centers through the halide atoms.[9]

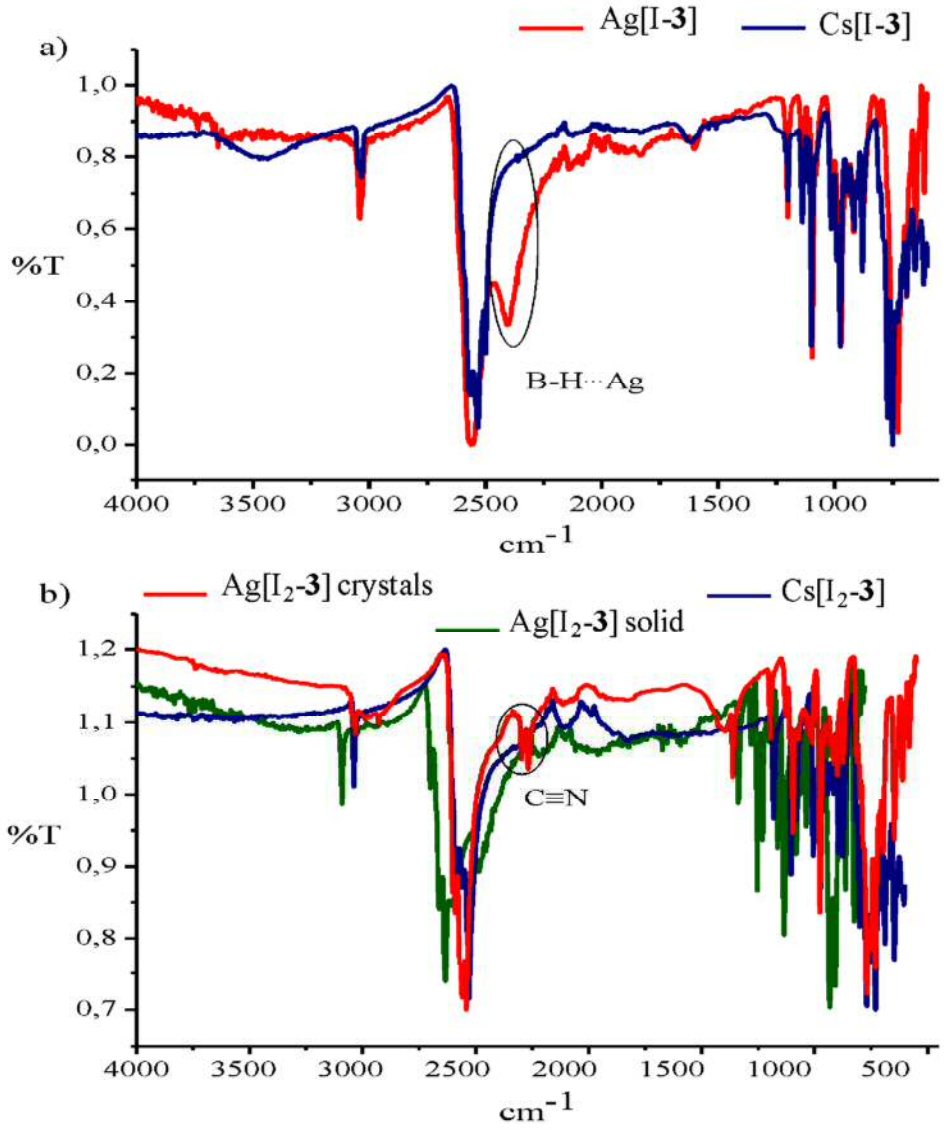

Figure 2.13. Comparison of IR spectroscopy between a) Cs[I-**3**] (blue) and Ag[I-**3**] (red); b) Cs[I_2-**3**] (blue), Ag[I_2-**3**] solid (green) and Ag[I_2-**3**] crystals (red).

The preparation of the silver salts of the anions [**3**]$^-$, [I-**3**]$^-$ and [I_2-**3**]$^-$ was achieved by dissolving the cesium salts in EtOH : H_2O (1:1), followed by the addition of an aqueous solution of $AgNO_3$ until the silver complex fully precipitates. The orange complexes were filtered under vacuum and washed with water and hexane. The

complexes were characterized by spectrometric and spectroscopic techniques as NMR, IR, MALDI-TOF-MS spectroscopies and X-ray diffraction in some cases.

By overlapping the two IR spectra of Cs[I-**3**] and Ag[I-**3**] (Figure 2.13a), one can see that the only difference that appear is the stretching band at 2400 cm^{-1} in the silver complex that can be attributed to the Ag···H-B interaction.

From the IR spectra represented in Figure 2.13b, the spectrum of the powder Ag[I_2-**3**] presents stretching B-H bands at 2399, 2368, 2344, 2325 cm^{-1} that disappear in the spectrum of Ag[I_2-**3**] of the crystals form in acetonitrile. The B-H bands of these crystals are comparable to the frequencies of B-H of the Cs[I_2-**3**] but the 2 bands that appear at 2297 and 2267 cm^{-1} in the silver complex correspond to the CN group of acetonitrile used in the crystallization process.

The B-H stretching of cobaltabis(dicarbollide) derivatives is found as a very intense broad band near 2550 cm^{-1} in IR spectra. This broad band is often split into several well-resolved peaks. This splitting can, in favorable situations, be used to draw information about non-equivalent B-H bonds, thus treating the IR bands as NMR signals. The natural abundance of ^{10}B and ^{11}B isotopes must lead to the broadening of the vibrational bands in the IR spectra of 1,2-*closo*-C_2B_{10} derivatives, corresponding to the motions in which boron atoms participate. The rigidity of the cluster in cobaltabis(dicarbollide) is the reason for the absence of low-frequency modes in IR spectra.[10]

The stretching and bending C_c-H and B-H modes in cobaltabis(dicarbollide) derivatives are very useful. If the two C_c-H bonds in a cobaltabis(dicarbollide) derivative become non-equivalent as for asymmetric B vertexes substitution in [I-**3**]$^-$, two stretching bands, $\nu(C_c\text{-H})$, with different frequencies and intensities may be expected in the IR spectrum. In the solid-state, the $\nu(C_c\text{-H})$ and ν(B-H) frequencies are extremely sensitive to the molecular structure as well as to intra- and intermolecular interactions.[11,12] If the C_c-H stretching frequency is measurably lower than 3040 cm^{-1}, that corresponds to the unsubstituted parent cluster, then it is fully consistent with the existence of H-bonding in the solid-state, presumably of the C_c-H···X type.

The ν(B-H) can also bring information on the ability of the B-H vertexes to participate in B-H···M agostic interactions. Agostic interactions are classified as covalent intramolecular interactions between a metal and a σ-bond [13] in close geometrical proximity to the metal atom. C–H···M agostic interactions are relatively

common and provide very important stabilization of transition metal compounds.[14] While the classic cases involve CH σ-bond close to early transition metals like titanium, many more agostic systems have been proposed which contain CH, SiH, BH, CC and SiC bonds coordinated to a wide range of metal atoms.[15] The geometrical parameters from crystal structures have provided good indication that an agostic interaction is present.[16] However, many approaches have been used to investigative the presence of an agostic bond; our group previously correlated the presence of agostic bonds by means of ^{1}H- and ^{11}B-NMR spectroscopy in solution.[17]

To the best of our knowledge, no correlation between the ν(B-H) and the presence of B-H···M agostic interactions has been reported till nowadays. If the stretching B-H frequencies become more energetic, this is fully consistent with the strengthening of the B-H bonds probably due to a complex combination of electronic effects and intermolecular interactions in the solid state. The IR spectrum of Ag[**3**] shows very strong frequencies of B-H bonds at 2576 and 2550 (B-H) and also bands at 2454 and 2384 cm^{-1}. It is important to focus on the latest ones because are the ones related with B-H···Ag interactions.

Interestingly, meticulous search in the literature and in the Cambridge Structural Database (CSD, Version 5.32) [18] revealed only three compounds with an Ag coordination centre exclusively formed by four B-H···Ag interactions and an extra ligand to originate five coordinated centres: $(C_{29}H_{25}P)[Ag(B_{12}H_{12})]$ and $(C_{29}H_{25}P)[Ag_2(B_{12}H_{12})_2MeCN]$ (where $C_{29}H_{25}P^+$ is the (1-naphthylmethyl)triphenylphosphonium cation), $[Ag_4(NC(CH_2)_2CN)_5(CB_{11}H_{12})_4]$9 and $(C_{13}H_{22}N)[Ag_3(B_{12}H_{12})_2(MeCN)_2]$ (where $C_{13}H_{22}N^+$ is benzyltriethylammonium cation).[19]

Recently, uncommon silver coordination environments occupied exclusively by B-H··Ag interactions, namely $(B\text{-}H)_4\cdots Ag$ and $(B\text{-}H)_6\cdots Ag$ centres, were observed in two coordination polymers of cobaltabis(dicarbollide), which is considerably larger than $B_{12}H_{12}^{2-}$ or $[CB_{11}H_{12}]^-$. [20] These polymers, [Ag(pim)(cobaltabis(dicarbollide)]

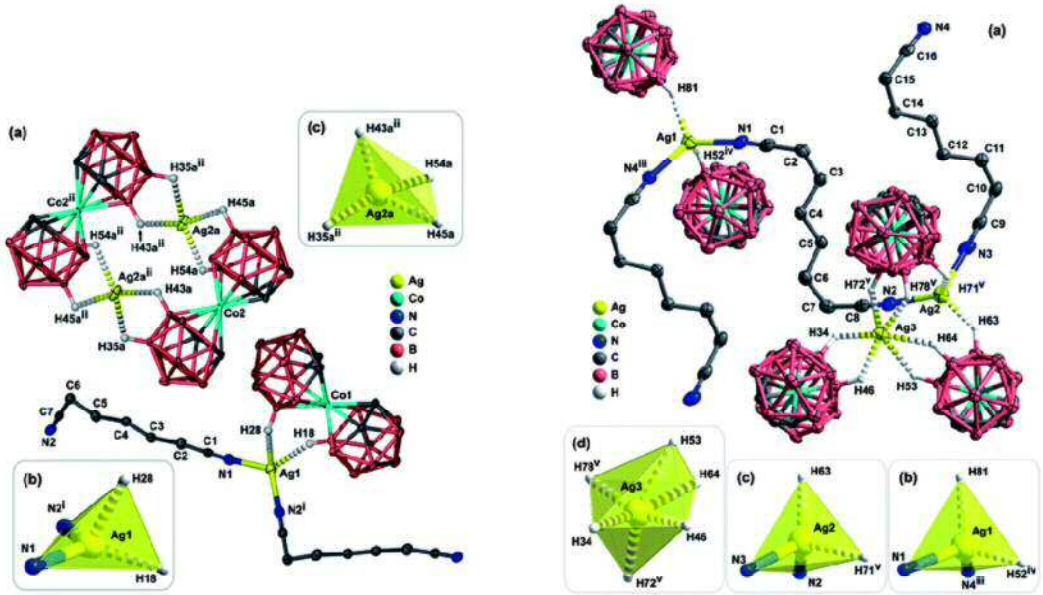

Figure 2.14. The 1D coordinated polymer showing the $(B\text{-}H)_4\cdots Ag$ interactions (left). The 2D coordination network displaying the $(B\text{-}H)_6\cdots Ag$ interactions (right).[22]

[Ag(Cobaltabis(dicarbollide))] (pim= pimelonitrile, $CN(CH_2)_5CN$) and $[Ag_3(sub)_2$(Cobaltabis-dicarbollide], are shown in Figure 2.14. Both complexes exhibit Ag centres that are purely coordinated by B-H···Ag interactions, namely $(B\text{-}H)_4\cdots Ag$ for the first 1D coordinated polymer and $(B\text{-}H)_6\cdots Ag$ for the second 2D coordination network. Both B-H···Ag interactions are a highly uncommon coordination motif and it is reported that their IR spectra display B-H frequencies at 2561 (s), 2411 (w), 2329 (w), 2275 (w) and 2538 (s), 2392 (s), 2286 (m) for [Ag(pim)(cobaltabis(dicarbollide)] [Ag(Cobaltabis(dicarbollide))] and $[Ag_3(sub)_2$(Cobaltabis-dicarbollide], respectively.

The IR spectra of Ag[**3**], Ag[I-**3**] and Ag[I_2-**3**] compounds display ν(B-H) at 2454 and 2384 cm^{-1} while the IR spectrum of crystals of Ag[I_2-**3**] does not show (see Figure 2.13). If the strengthening of the B-H bonds is due to intermolecular interactions in the solid state, the crystal structure of Ag[I_2-**3**] should not present B-H···Ag interactions. To prove it, crystals suitable for X-ray diffraction of Ag[I_2-**3**] were grown

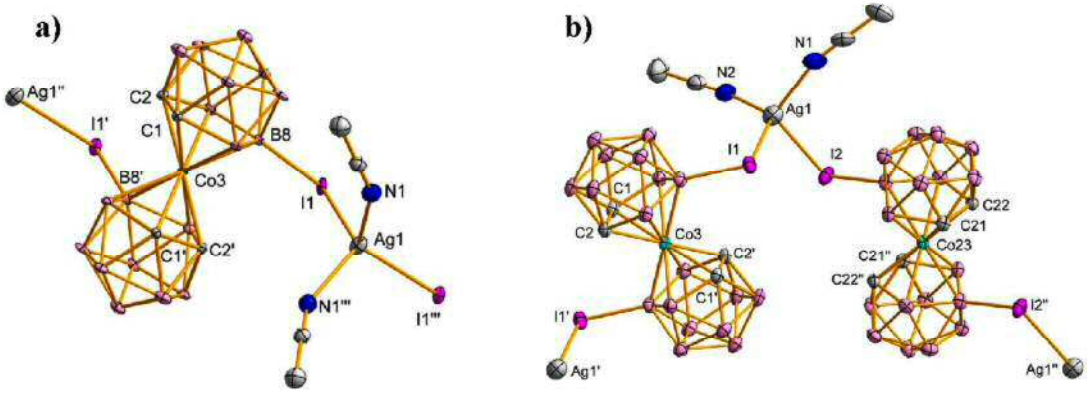

Figure 2.15. Basic structural units of Ag[I_2-**3**]: **a)** form on the left and **b)** on the right.

from a solution of acetonitrile (Figure 2.15a), and acetonitrile : isopropanol, 1:1, (Figure 2.15b).

Ag[I_2-**3**] = $[Ag(I_2\text{-}\mathbf{3})(CH_3CN)_2]_n$ crystallizes in two crystal forms (**a** – orthorhombic system and **b** - triclinic system): both are polymers. Figure 2.15 displays a basic structural part of both forms (**a** form on the left), in which Ag(I) ions have a distorted tetrahedral coordination sphere: two neutral I atoms and two N atoms coordinated to Ag(I) ion. In form **a** two Ag1-I1 and Ag1-N1 bonds are 2.7840(5) and 2.284(5) Å, respectively. In form **b,** Ag-I bonds are longer [2.8495(4) and 2.8778(4) Å]. The Ag-N bonds (form **b**) are 2.230(5) and 2.279(5) Å. In form **a,** the angles around Ag(I) are from 94.7(3)° (N1-Ag1-N1''') to 122.22(14)° (Ni1-Ag1-I1) and in form **b** they are from 101.497(14)° (I1-Ag1-I2) to 124.75(11)° (N2-Ag1-I1). The coordination sphere of Ag(I) in form **a** is more distorted from tetrahedron than that one in form **b.**

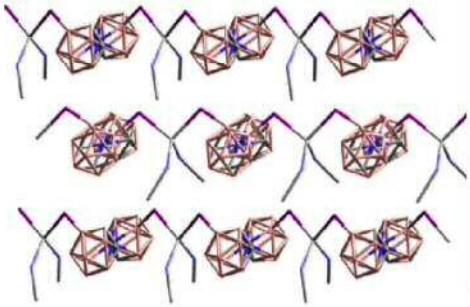

Figure 2.16. Polymerization of Ag[I_2-**3**] (form **a**) along *a* axis.

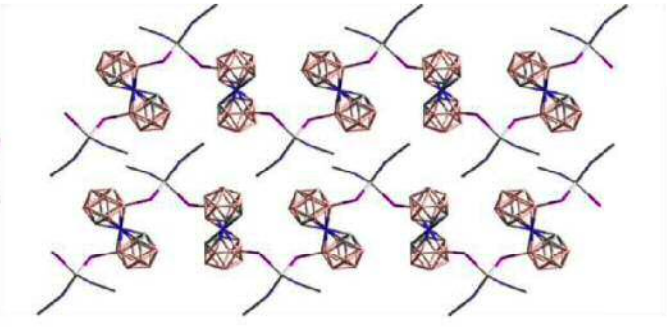

Figure 2.17. Polymerization of Ag[I_2-**3**] (form **b**) along the diagonal of *ac*-plane.

In form **a**, the I1···I1' distance in the boron cage is 6.2404(4) Å, but in form **b** there are two slightly different boron cages with the I1···I1' distance of 7.5455(5) and I2···I2'' distance of 7.4886(5) Å. The reason for two crystal forms is the position of I atoms coordinated to the Ag in form **a**, I atoms of the cobaltabis(dicarbollide) are in *cis* while in form **b** they are in *trans*.

Figure 2.16 displays the extended crystalline packing of Ag[I_2-**3**] (form **a**) grown in acetonitrile. The bridging nature of the iodine atoms between Ag centers results in the formation of 1D coordination polymers (linear chains), which expand along the *a*-axis of the unit cell, with I1···I1''' intra-chain distance being 4.1987(4) Å. The intra-chain Co and Ag atoms are on the same line with Co and Ag distances of 10.0506(2) Å.

The part of the crystal packing of Ag[I_2-**3**] (form **b**) grown in a mixture of acetonitrile - isopropanol (1:1) is shown in Figure 2.17. Also the iodine atoms bonded to B(8) and B28 bridge the Ag centers forming polymeric zigzag type chains that develop along the diagonal of *ac*-plane of the unit cell. The I1···I2 intra-chain distance being 4.4351(4) Å while the intra-chain Co atoms (Co3 and Co23) form a line with Co distances of 7.9437(3) Å. Unsymmetrical Ag1···Ag1'andAg1···Ag1'' distances are10.3925(7) and 12.0283(7) Å , respectively.

The Table 2.4, it is shown the characterization by $^{1}H\{^{11}B\}$-NMR, $^{11}B\{^{1}H\}$-NMR, $^{13}C\{^{1}H\}$-NMR and IR spectroscopies for the silver and cesium salt of [**3**]$^-$, [I-**3**]$^-$ and [I_2-**3**]$^-$. All the NMR spectra have been run in d^6-acetone.

Entry	δ ^{1}H-NMR C_c-H	δ ^{1}H-{^{11}B}-NMR B-H	δ ^{13}C{^{1}H}-NMR	υ (cm^{-1})	
				υ (C_c-H)	υ (B-H)
Cs[3]	3.96 (br s, 4H)	3.40, 2.99, 2.72, 1.95, 1.64, 1.59	51.03	3040	2576, 2530, 2508
Ag[3]	4.07 (br s, 4H)	3.56, 3.02, 2.85, 1.68, 1.64	51.95	3041	2576, 2550, 2454, 2384
Cs[I-3]	4.55 (br s,2H) 4.31 (br s,2H)	3.16, 3.04, 2.97, 2.60, 2.48, 1.95, 1.87, 1.79, 1.73	59.34 49.16	3041, 3033	2572, 2563, 2533
Ag[I-3]	4.36 (brs, 2H) 4.28 (br s, 2H)	3.17, 3.08, 2.91, 2.78, 2.13, 1.91, 1.80, 1.76, 1.68	55.09 50.75	3036	2565, 2550, 2402, 2376, 2337
Cs[I_2-3]	4.40 (br s, 4H)	3.23, 3.06, 2.82, 2.59, 2.14, 1.83	60.07	3040	2590, 2560, 2530
Ag[I_2-3]	4.51(br s, 4H)	3.24, 3.08, 2.93, 2.68, 2.13, 1.86	59.03	3040	2585, 2557, 2530, 2398, 2368, 2343

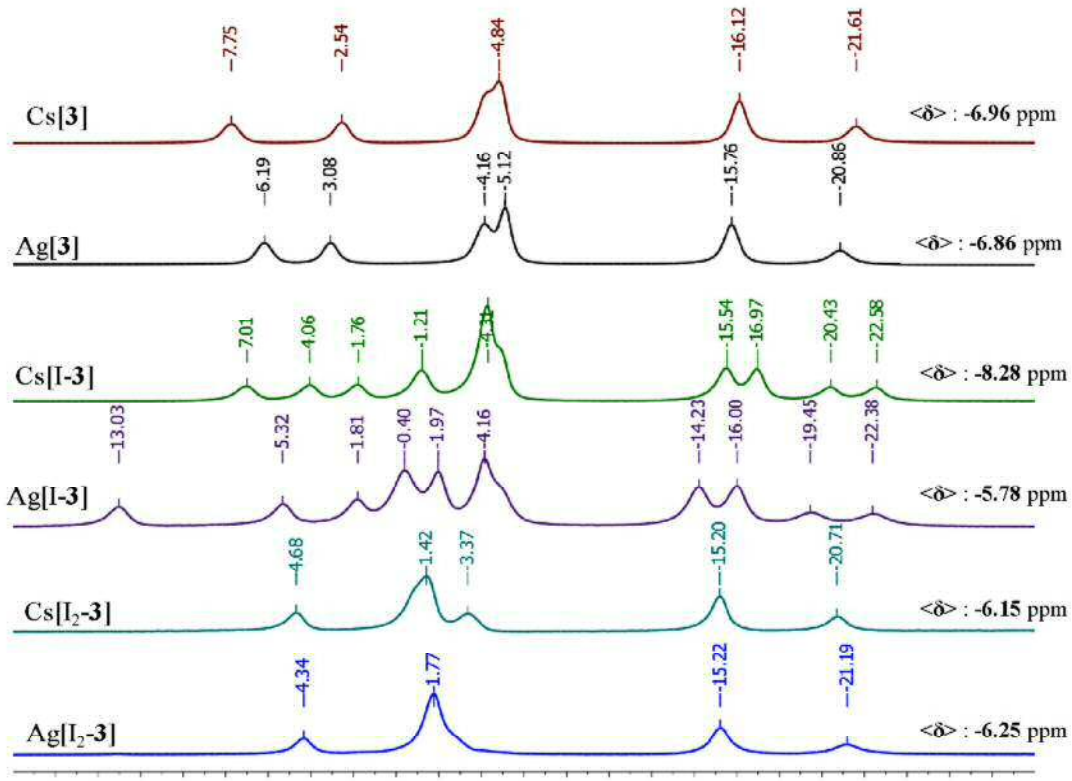

Table 2.4. ^{1}H-, ^{1}H{^{11}B}-, ^{13}C{^{11}B}-NMR chemical shift (in ppm) and IR stretching for the compounds: Cs[**3**], Ag[**3**], Cs[I-**3**], Ag[I-**3**], Cs[I_2-**3**] and Cs[I_2-**3**].

Cs[I-**3**], Ag[I-**3**], Cs[I_2-**3**] and Ag[I_2-**3**].

We also synthesized the silver salt of tetra and octaiodinated derivatives of cobaltabis(dicarbollide), Ag[I_4-**3**] and Ag[I_8-**3**], but we were not able to characterize them by NMR spectroscopy because solubility problems in ordinary solvent.

iii) Iron (II) and Iron (III) salts of cobaltabis(dicarbollide)

Silver set of cobaltabis(dicarbollide) derivatives were used as precursor to prepare the corresponding Fe(II) and Fe(III) salts.

In order to obtain the iron (II) and iron (III) salts of cobaltabis(dicarbollide), under a nitrogen atmosphere the silver salt was dissolved in the minimum volume of deoxygenated ethanol and either $FeCl_2$ or $FeCl_3$ was added in solid. Stoichiometric ratio was 1/2 or 1/3 for Fe(II) and Fe(III), respectively, as shown in Scheme 2.4. The white precipitate, AgCl, that was formed was discarded and the orange/brownish solutions were concentrated using a rotary evaporator. All the compounds were characterized by ^{1}H, ^{11}B, ^{13}C-NMR and FTIR spectroscopy as well as MALDI-TOF-MS.

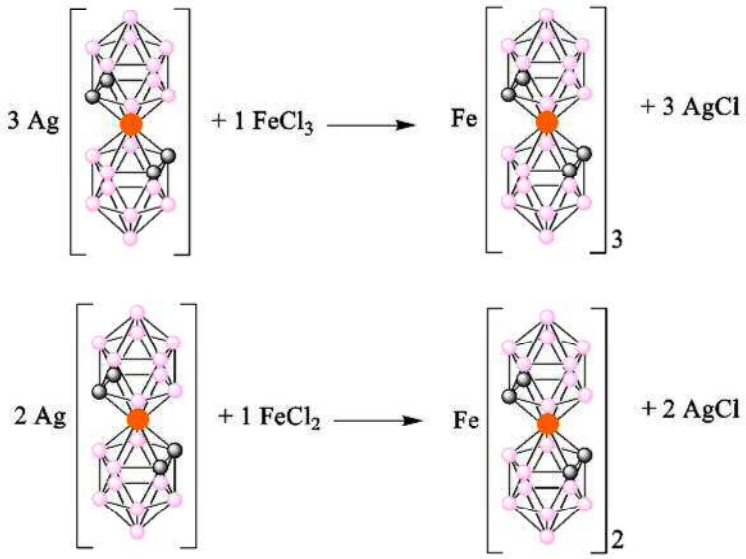

Scheme 2.4. Synthesis of iron salts of cobaltabis(dicarbollide), Fe[**3**]$_2$ and Fe[**3**]$_3$.

A comparison between the coupled ^{1}H-NMR spectrum (red) and the decoupled $^{1}H\{^{11}B\}$-NMR (blue) to the boron of Fe[**3**]$_3$ and Fe[**3**]$_2$ is illustrated in Figure 2.19.

In the decoupled spectrum, the signals of protons coupled to ^{11}B appear as broad singlets since the two isotopes of boron (^{10}B and ^{11}B) posses different spin numbers as well as different abundance. For ^{10}B s = 3 and abundance = 20% while for ^{11}B s= 3/2, and abundance = 80%. The signal that appears at the lowest field belongs to the H bonded to the carbon, the values are 3.96 ppm for Fe[**3**]$_3$ and 3.91 for Fe[**3**]$_2$.

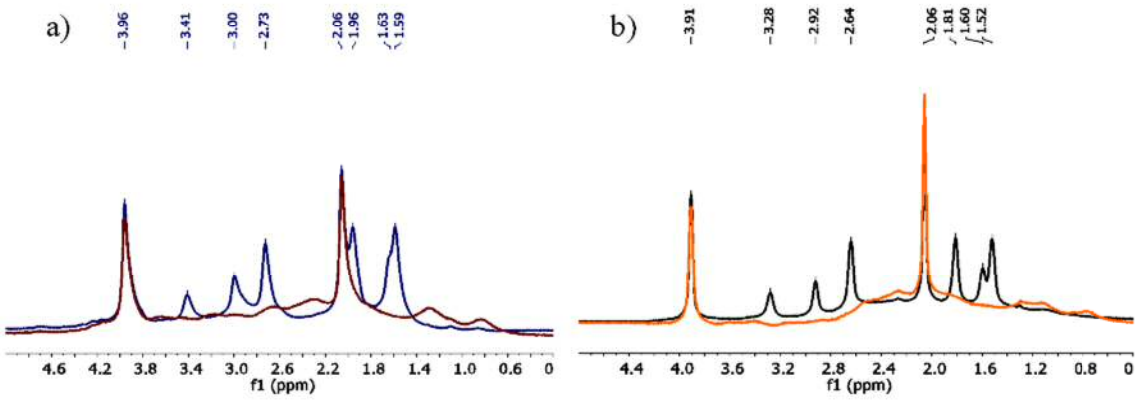

Figure 2.19. a) Comparison between ^{1}H-NMR (red) and ^{1}H{^{11}B}-NMR (blue) for compound Fe[**3**]$_3$; b) Comparison between ^{1}H-NMR (orange) and ^{1}H{^{11}B}-NMR (black) for compound Fe[**3**]$_2$.

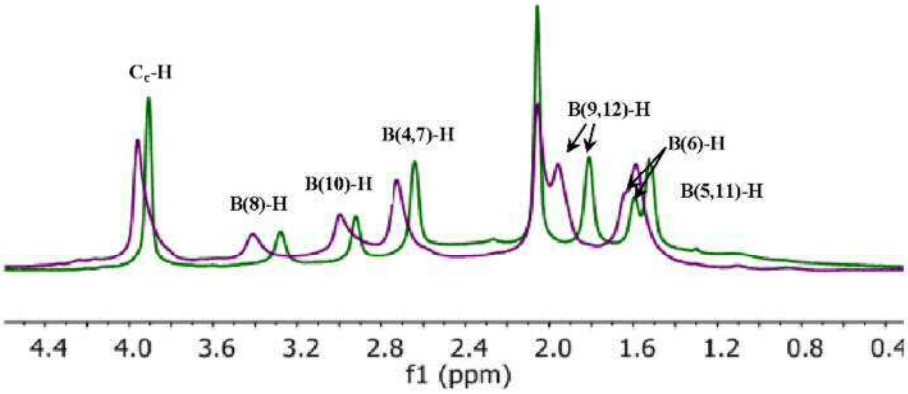

Figure 2.20. ^{1}H{^{11}B}-NMR comparison between Fe[**3**]$_2$ (green) and Fe[**3**]$_3$ (purple).

By overlapping the ^{1}H{^{11}B}-NMR spectra of Fe[**3**]$_2$ and Fe[**3**]$_3$ compounds, one can observed that the proton resonances of the paramagnetic Fe[**3**]$_3$ species were shifted to downfield compared to the chemical shift of the signals that correspond to the diamagnetic Fe[**3**]$_2$. The most affected proton atoms of the Fe[**3**]$_3$ are the ones bonded to B(9,12) and B(8).

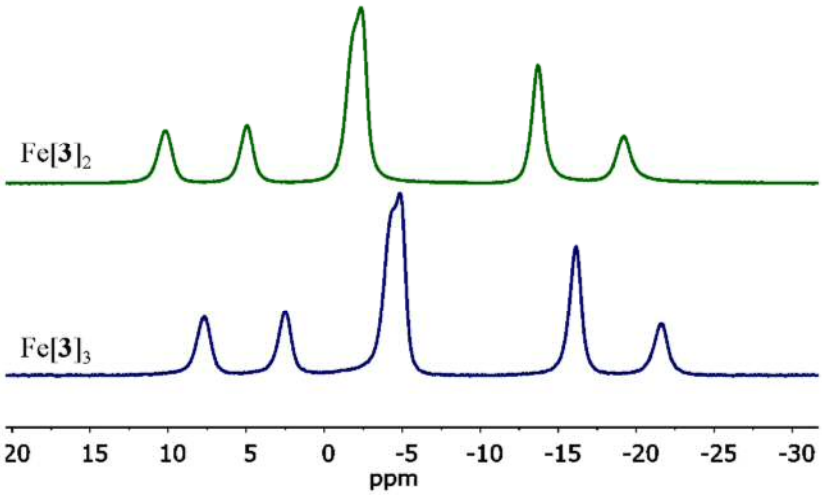

Figure 2.21. Comparison of ^{11}B-NMR spectra of the Fe[**3**]$_2$.(green) and Fe[**3**]$_3$ (blue).

The $^{11}B\{^1H\}$-NMR spectra of the diamagnetic species Fe[**3**]$_2$ and the paramagnetic Fe[**3**]$_3$ display similar pattern but the full spectrum of the paramagnetic species is shifted up field with respect to the diamagnetic one. The influence of the paramagnetic Fe^{3+} in $Fe[Co(C_2B_9H_{11})_2]_3$ produces a noticeable but small effect on the ^{11}B spectrum of the compound. It will be seen in the Section 2.1.3 that the effect of the paramagnetic Fe^{3+} in the anionic $[Fe(C_2B_9H_{11})]^-$ cluster produces a very large impact in its ^{11}B-NMR spectrum. To be noticed that Fe^{3+} is η^5 bonded to the anionic [**4**]$^-$ compound.

2.1.2.b.- Chlorinated derivatives

Although the [3,3'-Co-(1,2-$C_2B_9H_{11})_2]^-$ is extremely stable, several mild conditions afford halogenation.[21] The reported synthesis of chlorinated derivatives of Cs[3,3'-Co-(1,2-$C_2B_9H_{11})_2]^-$ was based on the reaction of Cl_2 with Cs[**3**]; this reaction produced mixtures of complexes with several Cl atoms ranging from 2 to 6.[22] On the other hand pure [$NHMe_3$][Cl_2-**3**] was reported to be synthesized by reaction of *N*-chlorosuccinimide with [$NHMe_3$][**3**] in THF.[21] Also, chlorination of [NMe_4][**3**] by hypochlorous acid is unique in that the reaction gives exclusively B(8), B(8')-disubstitution [Cl_2-**3**]$^-$ and does not produced to further substitution at room temperature.[21] Few years later, the electrochemical synthesis of the [NMe_4][Cl_2-**3**] was published with a reasonable yield of 42.7%.[23]

The reactivity of the different vertexes B-H is different. So, it has been shown by computational studies[24] that the chlorination would take place first on B(8), and then, without any preference, on B(9,12) and B(10) follow by B(4,7) and B(5,11). The last preferential chlorination site in the cluster is on B(6) because these boron is connected directly with both C_c, being the least electronic vertex.

Although cobaltabis(dicarbollide) itself is reasonably stable, the chlorinated derivatives have shown even greater stability in acidic media. For example, the six chloro derivative is the most relevant in radionuclide separation.[25] This has surfactant properties[26,27] and high stability in highly acid media.[28] Multiply chlorinated derivatives of the cobaltabis(dicarbollide) anion have been tested in solutions of 3 M nitric acid, with less than 5% decomposition even after 36 days, compared to 80% decomposition of the parent cobaltabis(dicarbollide) anion under the same conditions.[21]

In 2010, our group, developed a useful method to increase the chlorination degree of cobaltabis(dicarbollide) by reacting *N*-chlorosuccinimide with Cs[**3**] in the oven at 200(±6) ºC in a vaccum sealed tube.[29] The characterization by MALDI-TOF MS gives the chemical composition of the studied samples. It was found mixtures of anions. The most chlorine enriched derivative produced was with 9 chlorine.[29]

In the case of the [$NHMe_3$][**3**] using 2.3 eq. of *N*-chlorosuccinimide in THF, the disubstituted chlorine derivative, was completely obtained in 20 minutes by heating.[21]

When we tried this synthesis starting with Cs[**3**], it took more than 4 h refluxing and overnight stirring at room temperature. If the number of equivalents of *N*-chlorosuccinimide is increased from 2.3 to 12, the MALDI-TOF-MS spectrum showed a mixture of 4 chlorinated species: disubstituted (6.98%), trisubstituted (46.79%), tetrasubstituted (38.17%) and pentasubstituted (8.06%).

We changed the chlorinated agent by using sulfuryl chloride (SO_2Cl_2). Compared to other chlorinated agents, SO_2Cl_2 is inexpensive, less hazardous to handle in the laboratory under safety precautions and more amenable to use on different reaction scales.

Refluxing for 2 hours, Cs[**3**] with mixture of SO_2Cl_2 and THF (1:1) we obtained a mixture of tetrasubstituted (28.19%), pentasubstituted (52.95%) and hexasubstituted (18.86%). After 19 hours we got the tetrasubstituted (17.39%), pentasubstituted (37.98%), hexasubstituted (30.14%) and heptasubstituted (14.49%).

Another trial was to change the THF with acetonitrile, because we wanted to increase the temperature of the reaction. Boiling point of acetonitrile is 82 °C comparing with 66 °C for THF.

The reaction of 50 mg of Cs[**3**] with a mixture of SO_2Cl_2 and acetonitrile (1:1) for different time led to a partially chlorinated [3,3'-Co($C_2B_9H_{11-y}Cl_y$)($C_2B_9H_{11-z}Cl_z$)]

Entry	Time	[3,3'-Co($C_2B_9H_{11-y}Cl_y$)($C_2B_9H_{11-z}Cl_z$)]						
		x = 5	x = 6	x = 7	x = 8	x = 9	x = 10	x = 11
1	86 h at room temperature	**23.93**	**50.20**	**21.23**	**4.63**			
2	45 min, 70°C	**28.13**	**65.81**	**6.06**				
3	1 hour, 70°C	**25.95**	**64.69**	**9.36**				
4	2 hours, 70°C	**10.52**	**72.74**	**16.74**				
5	4 hours, 70°C	**4.3**	**55.64**	**35.76**	**4.3**			
6	16 hours, 70°C		**25.46**	**60.19**	**14.35**			
7	46 hours, 70°C		**8.72**	**57.46**	**31.55**	**2.27**		
8	70 hours, 70°C		**2.69**	**38.32**	**45.53**	**11.97**	**1.49**	
9	85 hours, 70°C			**32.40**	**52.97**	**12.89**	**1.74**	
10	92 hours, 70°C			**25.89**	**57.05**	**15.19**	**1.87**	
11	116 hours, 70°C			**19.36**	**56.63**	**20.85**	**3.16**	
12	147 hours, 70°C			**11.02**	**53.75**	**30.25**	**4.98**	
13	180 hours, 70°C			**11.56**	**47.05**	**30.98**	**9.49**	**0.92**

Table 2.5. Percentage of the mixture of chlorinated derivatives of cobaltabis(dicarbollide) as a function of time. x=y+z, x is the total number of chlorine atoms exchanged for hydrogen atoms in Cs[**3**].

based on MALDI-TOF-MS evidence. After every 2 days of heating, we evaporated the solvent and fresh mixture of SO_2Cl_2 : acetonitrile (1:1) was added. Table 2.5 displays the percentage of the mixture of chlorinated derivatives [Cl_x-**3**]$^-$ as a function of time.

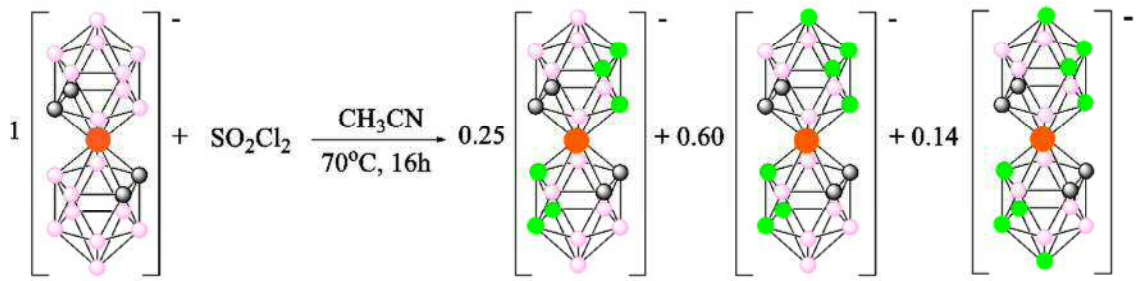

Scheme 2.5. Schematic representation for the entry 6.

Previously, our group demonstrated that the preferential chlorination sites on [**3**]$^-$ were not of thermodynamic origin but, similarly to aromatic substitution, the preferential chlorination sites in cobaltabis(dicarbollide) anion are of kinetic origin.[24] As a mixture of compounds were obtained with the chlorination reaction of the [**3**]$^-$ cluster by using N-chlorosuccinimide, it was required to find a fast, reliable, and quantitative analyzing method. The mass spectroscopic technique MALDI-TOF-MS was the most suitable one to analyze monoanionic boron clusters.[29,30] Recognizing that the technique provides information on the individual mass of each distinct component of the analyzed sample, but not on the possible positional isomers that may exist in each individual mass, we refer to a particular m/z signal or signal envelop as a 'compound'. This may consist of several positional isomers. One example of the reaction is exemplified in Scheme 2.5 for [**3**]$^-$ with mixture of SO_2Cl_2 and acetonitrile (1:1) at 70°C during 16 h. There are several parameters that can be retrieved from the data in Table 2.5: the reaction running for 86h at room temperature produces four chlorinated derivatives ([Cl_5-**3**]$^-$, [Cl_6-**3**]$^-$ and [Cl_7-**3**]$^-$). At 70°C in the interval of 45 minutes – 2 hours, the hexachlorinated [Cl_6-**3**]$^-$ is the most abundant. At 70°C for 4 hours, the hexachlorinated [Cl_6-**3**]$^-$ is still the most abundant but the octachlorinated [Cl_8-**3**]$^-$ compound starts to be obtained. At 70°C in the range 46 - 72 hours, the nonachlorinated [Cl_9-**3**]$^-$ compound starts being obtained. While, after 70 hours, the decachlorination, [Cl_{10}-**3**]$^-$, take place. To notice that the highest chlorinated [Cl_{11}-**3**]$^-$ species is detected in a very little amount after 180 hours at 70°C.

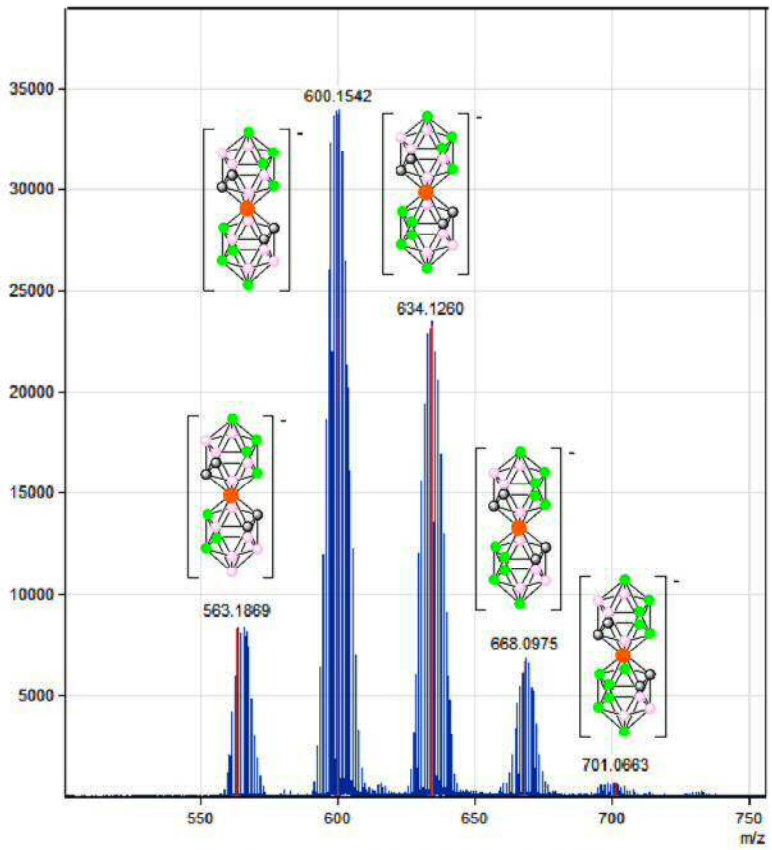

Figure 2.22. Negative MALDI-TOF-MS spectrum after 180 hours for cobaltabis(dicarbollide).

2.1.3.- Anionic ferrabis(dicarbollide) derivatives

Since the ferrabis(dicarbollide) compounds are Fe(III) paramagnetic species, paramagnetic shifting with respect to the corresponding diamagnetic cobaltabis(dicarbollide) derivatives should be expected in the NMR spectra.[31,32] This is why precautions regarding the extent of the spectral window have to be taken when running ^{1}H and ^{11}B NMR.

The paramagnetic character of Fe(III) enlarges the spectral range of the $^{11}B\{^{1}H\}$-NMR spectrum of [3,3'-Fe($C_2B_9H_{11}$)$_2$]$^-$, [**4**]$^-$, with respect to the diamagnetic [3,3'-Co($C_2B_9H_{11}$)$_2$]$^-$, [**3**]$^-$, from 30 ppm to 550 ppm (Figure 2.23). Likewise, the same paramagnetic character prevents the observation of the $^{1}J(^{11}B, ^{1}H)$ coupling between the B and the H nuclei in the ^{11}B NMR spectra (Figure 2.24a and 2.24b, right).

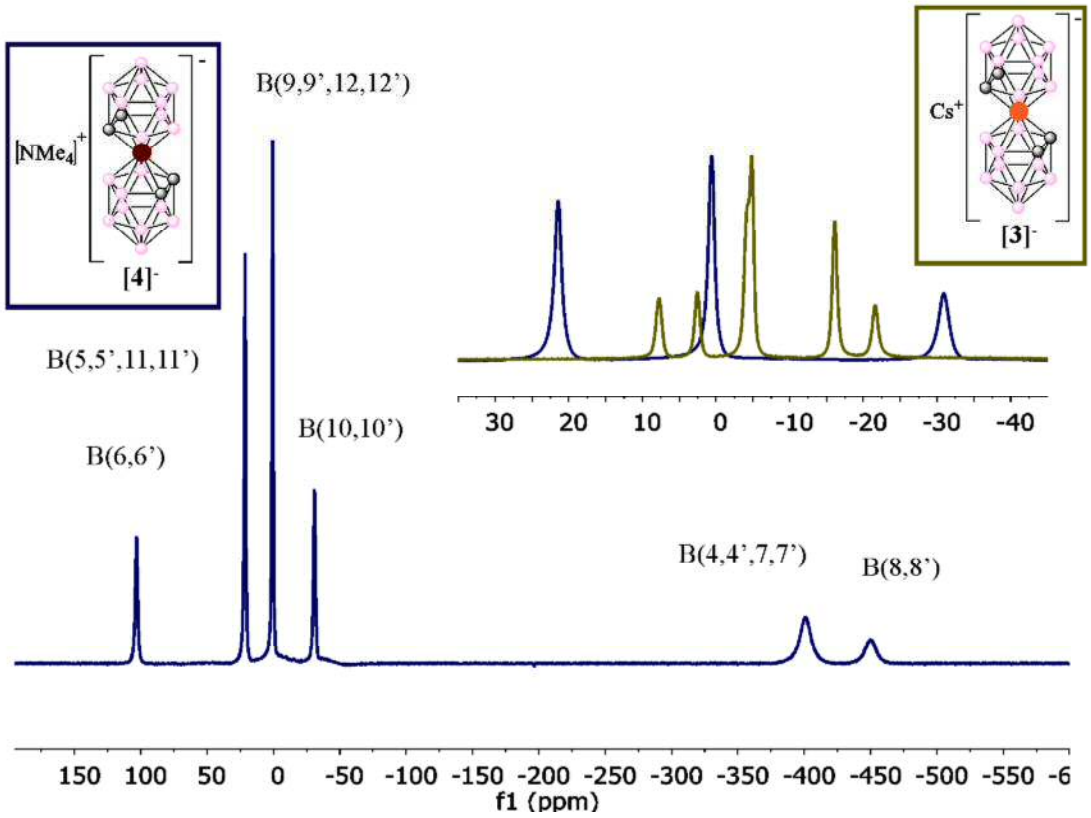

Figure 2.27. $^{11}B\{^{1}H\}$-NMR spectra of the paramagnetic $[NMe_4]$[**4**] (blue) and its spectrum magnification in the range +35/-30 ppm for comparison with Cs[**3**] (green)

As depicted in Figure 2.24b, the ^{11}B NMR spectra of zwitterionic monosubstituted, **5** and **6**, species show the splitting of each signal present in the anionic parent metallabis(dicarbollide) cluster into two peaks due to the presence of two symmetrically inequivalent dicarbollide moities. Chart 2.1 displays the dicarbollide vertexes numbering and the symmetry plane of the ligand that is perpendicular to the C_2B_3 face and bisects the C_c-C_c bond.

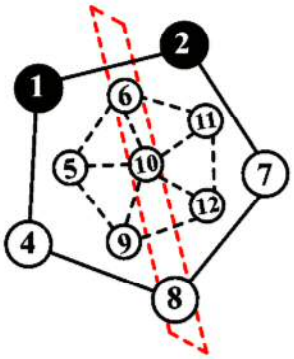

Chart 2.1. Projection and numbering of the dicarbollide unit.

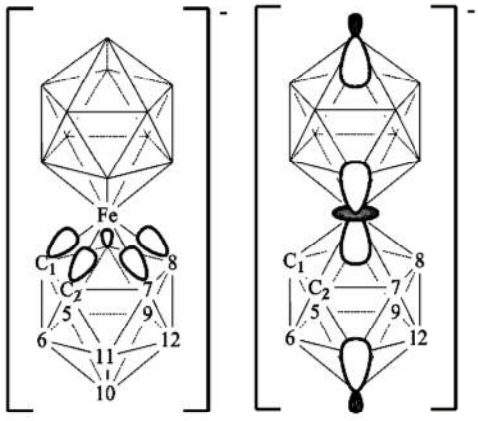

Chart 2.2. Symmetry adapted orbital interactions that describe the two sets of boron vertices that interact with Fe(II).

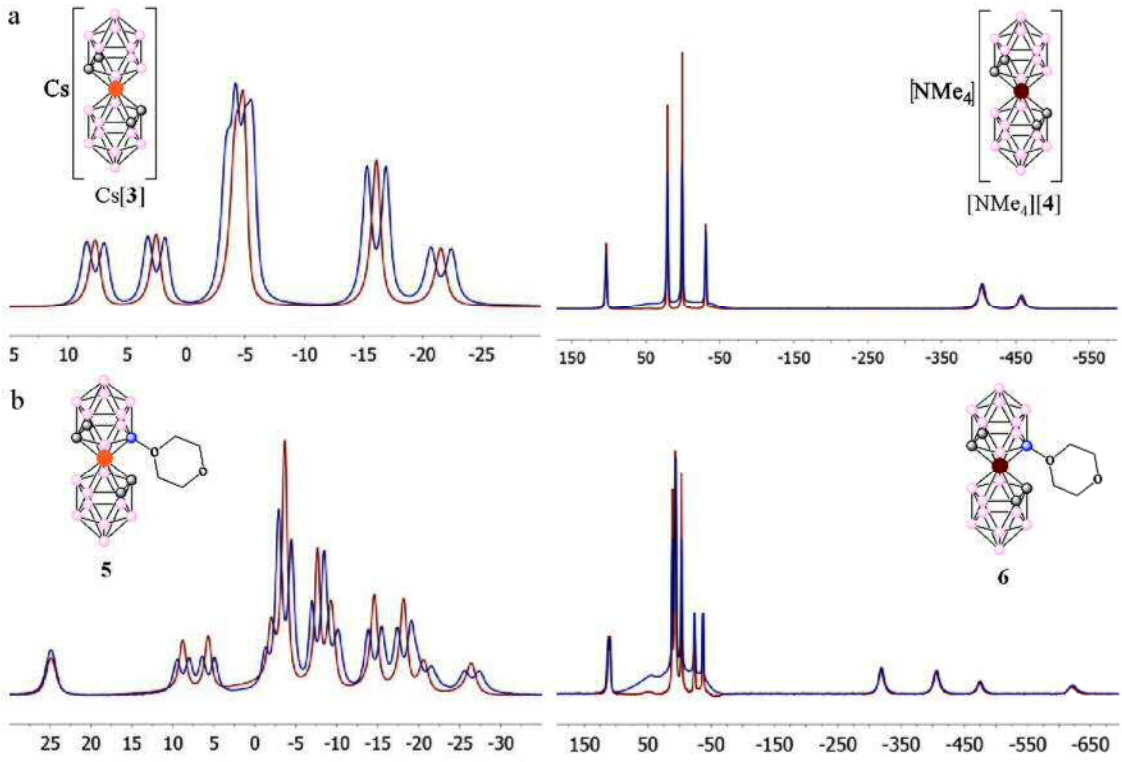

Figure 2.24. Comparison between experimental $^{11}B\{^{1}H\}$-NMR (blue) and ^{11}B-NMR (red) for (a) Cs[**3**] and [NMe_4][**4**]; (b) their dioxanate zwitterionic derivatives, **5** and **6**.

Additionally, in the case of [**4**]$^-$, the ^{11}B NMR spectrum (Figure 2.23) allows to identify the boron atoms most affected by the presence of the Fe(III) centre: the one that resonates at the lower field (≈+110 ppm) and the ones that appear at high field values (≈ -400 and ≈ -450 ppm). To note is that the areas peak pattern is 1:2:1. From Chart 2.2, one can observe the symmetry adapted of the two sets of boron vertexes that interact with Fe(III): these belonging to the η^5 bonding C_2B_3 face (B(8), B(4) and B(7)) and the one antipodal to the Fe(III) vertex, B(10). The symmetry plane of the ligand that is perpendicular to the C_2B_3 face and bisects the C_c-C_c bond, gives rise to two types of boron atoms in the η^5 bonding C_2B_3 face: on one hand, B(8) and on the other hand, B(4) and B(7), which are equivalent. So, it is expected that the three boron atoms on the C_2B_3 face, equally bonded to the Fe(III), will be affected in the same way, resonating close to one another, and showing a 2:1 peak pattern. So, presumably, B(8), B(4) and B(7) from the C_2B_3 face should be assigned at the highest field and B(10) vertex that is antipodal to Fe at the lowest field (Figure 2.23).

For diamagnetic metallabis(dicarboranes), the main variations occur also at the positions adjacent to the metal center, B(8), B(4), B(7) and at the metal-antipodal vertex B(10). Note that in the diamagnetic species all these boron vertexes move to lower field.[33] The assignment of the peaks suggested above was performed by $\{^{11}B\text{-}^{11}B\}$ COSY NMR of the paramagnetic [**4**]$^-$ species.[34] The extremely deshielded peak, appearing at the lowest field values (≈ +110 ppm), can be either the antipodal atom to Fe(III), B(10), or the boron atom connected to both carbon atoms, B(6). The $\{^{11}B\text{-}^{11}B\}$ COSY NMR spectrum does not discern between the B(10), B(6) assignment but the following two facts: i) the interactions of B(6) with other boron skeletal atoms are weak in diamagnetic metalladicarboranes[33b] and ii) the reported theoretical calculations data by using density-functional theory (DFT)[35] suggest assigning as B(6) the resonance at the lowest field. Then, the resonances assignments of the Boron vertexes in [**4**]$^-$ spectrum are as indicated in Figure 2.23.

$^{13}C\{^1H\}$ NMR spectrum of Cs[**4**] appears at -440 ppm that is 491 ppm upfield with respect to the C_c atoms of the diamagnetic Cs[**3**]. From Table 2.6, it is clear when

	δ Cs[**3**]		δ Cs[**4**]
$^{11}B\{^1H\}$-NMR	+ 6.5	B(8), B(8')	−451.1
	+ 1.4	B(10), B(10')	−30.9
	- 6.0	B(4), B(4'); B(7), B(7')	−402.4
	- 6.0	B(9), B(9'); B(12), B(12')	+21.8
	-17.2	B(5), B(5'); B(11), B(11')	+0.7
	-22.7	B(6), B(6')	+103.6
$^{13}C\{^1H\}$-NMR	51.0	C_c	−440.2
^1H-NMR	3.94	C_c–H	+45.04
$^1H\{^{11}B\}$-NMR	3.37, 2.93, 2.69 1.91, 1.57	B–H	+69.29, +40.72, +1.33, +3.14, −7.95

Table 2.6. $^{11}B\{^1H\}$, $^{13}C\{^1H\}$, ^1H and $^1H\{^{11}B\}$ chemical shifts (in ppm) for [**3**]$^-$ and [**4**]$^-$ in d^6-acetone.

comparing with the diamagnetic Cs[**3**] complex that the paramagnetic nature of the Fe(III) in the Cs[**4**] species mainly affects the chemical shift of the η^5 bonding atoms of the C_2B_3 face (B(8), B(4), B(7) and C_c atoms). Often scientists have wondered about the effects on the NMR spectra of a paramagnetic metal ion within a molecule. We have found that the two pristine systems that are used in this thesis are outstanding to answer this question, as it has been possible to quantify the extent of the paramagnetic ion

influence in neighboring atoms. Furthermore, it has been possible to quantify the influence on two distinct elements, B and C, and the results are consistent, even though two distinct NMR techniques have been necessary for the quantification. Thus it has been found that in the [**4**]$^-$ species all C_2B_3 face nuclei move upfield with regard to [**3**]$^-$: B(8) atoms resonate 44062 Hz upfield, as do B(4)/B(7) that shift 38157 Hz whereas C_c shift 36840 Hz, also upfield under a magnetic field of 7.05T.

The ^{1}H NMR spectrum of Cs[**4**] displays two broad signals at +69.29 and +40.72 ppm and a sharp singlet at +45.04 ppm. It was proved by bidimensional {^{1}H-^{11}B} HETEROCOSY NMR spectrum[34] that the resonance +45.04 corresponds to the H atoms bonded to C_c within the [**4**]$^-$ molecule. On the other hand, the sharp proton peak at +45.04 ppm interacts only with the peak previously assigned as B(10).

Silver salt of [4]$^-$

The silver salt of [**4**]$^-$ has been obtained by mixing the water solution of Na[**4**] with $AgNO_3$ in solid. The brown precipitate was rinsed with water and dried under vaccum. Ag[**4**] has been characterized by NMR and IR spectroscopies. In solid state, the IR spectrum display ν(B-H) at 2549 and 2384 cm^{-1}, that confirm the intermolecular interactions B-H···Ag. We dissolved the complex in d^6-acetone to run the NMR but we observed the formation of a precipitate. The NMR of the solution, showed some extra pics that approve the partial decomposition of the complex.

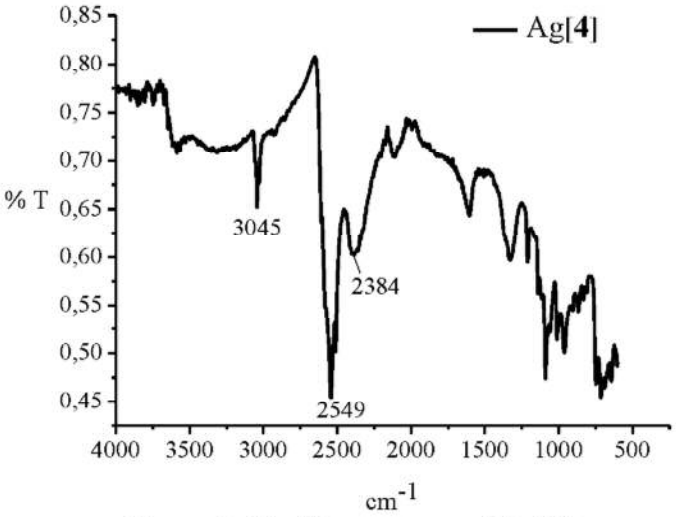

Figure 2.25. IR spectrum of Ag[**4**].

We observed that acetonitrile was a better solvent for characterization and also crystallization. Crystals suitable for X-ray diffraction were grown at room temperature. As it is shown in Figure 2.26, the refined structure surprised us at the beginning because the silver cation was not found. In a previous thesis in our group,[36] when carrying on the synthesis reaction of [**4**]$^-$ from the ligand [**2**]$^-$ and $FeCl_2$ in solid state also unexpected

results were obtained: not only the expected sandwich-type [**4**]$^-$ compound was obtained, but even substitute some hydrogen atoms for chlorine atoms on the complex. This information was extracted from the MALDI-TOF-MS. The mass spectrometry display 4 chlorinated compounds that are present within the mixture; the molecular peaks at 320 (63 %), 354.7 (18 %), 388.7 (12 %) and 466.9 (6 %) cm^{-1}, confirming the presence in a different proportion of the parent [**4**]$^-$, monochlorinated, dichlorinated and tetrachlorinated derivatives, respectively. The explanation was that probably chlorination of the positions B(8) and B(10), the former because since it is one of the boron atoms situated further from the carbon atoms, therefore bearing a more negative charge, and the latter because of the superposition of the hybrid *p* orbitals of both cobalt and B(10), had taken place.

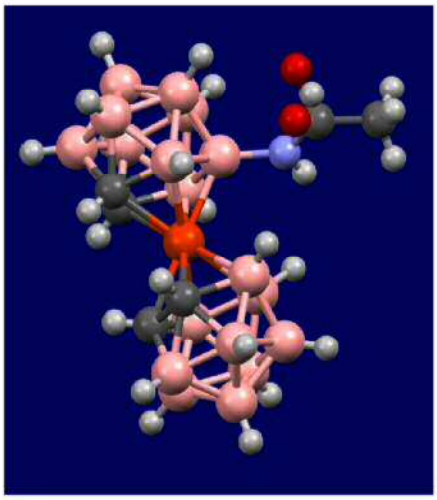

Figure 2.26. Crystal structure of the unexpected [**4**]$^-$ derivative.

Nevertheless, this chlorination phenomenon does not occur for the cobaltabis(dicarbollide), clearly showing the more reactive character of the iron-based complex, that, once formed, undergoes electrophilic substitution, yielding the pluri-halogenated complex.

Considering the presence of ν(B-H) at 2384 cm^{-1} in the IR spectrum of Ag[**4**], the results found in the precedent thesis and the decomposition of the Ag[**4**] in acetone the

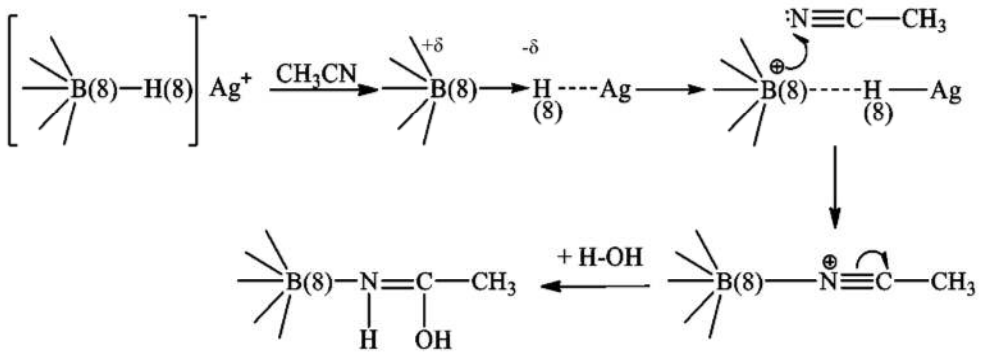

Scheme 2.6. Proposed mechanism.

explication of the crystal composition can be explained by the proposed mechanism displayed at Scheme 2.6.

2.1.3.a.- Iodinated derivatives

Following the procedure described for the synthesis of $[Me_8\text{-}\mathbf{3}]^-$ compound, the synthesis of $[I_4\text{-}\mathbf{4}]^-$ and $[I_8\text{-}\mathbf{4}]^-$ species were obtained as shown in Scheme 2.7. As an exemple, to a stirring solution of $[HNMe_3][I_2\text{-}\mathbf{2}]$ in THF cooled to 0°C in an ice-water bath was added, drop wise, a solution of buthyl lithium in hexanes to deprotonate the bridging proton of the *nido* $[I_2\text{-}\mathbf{2}]^-$. The suspension of the dianionic dicarbollide, $[I_2\text{-}\mathbf{2}]^{2-}$, was stirred for 1 hour at 0°C and 30 minute at room temperature. Volatiles were removed under reduced pressure. The complexation reaction of this ligand was achieved by transferring via a syringe of the resulting solution onto a $FeCl_2$ anhydrous solution in THF, following which the reaction was heated to reflux for 1.5 hours under nitrogen. The Fe(II) complex, $[I_4\text{-}\mathbf{4}]^{2-}$ was converted to the Fe(III), $[I_4\text{-}\mathbf{4}]^-$ by stirring the reaction

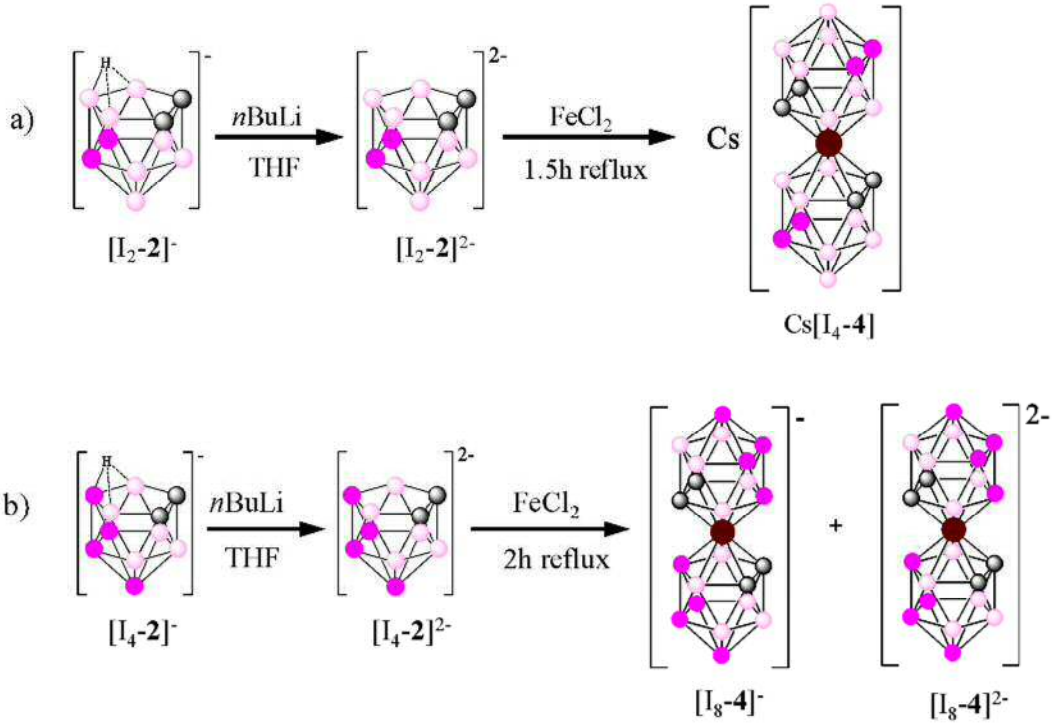

Scheme 2.7. a) Synthetic route for $Cs[I_4\text{-}\mathbf{4}]$; b) Synthetic route for $[I_8\text{-}\mathbf{4}]^-$/ $[I_8\text{-}\mathbf{4}]^{2-}$.

solution for 1hour in the presence of air. After evaporation of the solvent under vacuum, the resulting dark solid was extracted 3 times with diethyl ether/0.1 M HCl. The combined organic phase was dried over $MgSO_4$, filtered and the solvent removed under reduced pressure. Then the solid was dissolved in water and an aqueous solution of

saturated CsCl was added drop by drop until the paramagnetic Cs[I_4-**4**] species precipitate. The dark solid was filtered and rinsed with water obtaining the yield of 80%.

Starting from [I_4-**2**]$^-$, (Scheme 2.7b), the two species [I_8-**4**]$^-$/ [I_8-**4**]$^{2-}$ were also isolated as cesium salts.

δ Na[**4**]	δ Cs[I_4-**4**]	δ Cs[I_8-**4**]
104.72 (1B)	106.43 (1B)	120.07 (1B)
22.09 (2B)	10.46 (2B)	19.24 (2B)
0.65 (2B)	-30.52 (2B)	-0.08 (2B)
-30.83 (1B)	-55.01 (1B)	-109.94 (1B)
-405.52 (2B)	-429.83 (2B)	-337.70 (2B)
-454.35 (1B)	-493.97 (1B)	-500.80 (1B)

Table 2.7. $^{11}B\{^1H\}$ chemical shift (in ppm) for Na[**4**], Cs[I_4-**4**] and Cs[I_8-**4**] in d^6-acetone.

As it is observed in Table 2.7, the <δ> of the spectra of [**4**]$^-$ moves 11 ppm to high field in the tetraiodinated derivative [I_4-**4**]$^-$ and the <δ> of the spectra of [I_8-**4**]$^-$

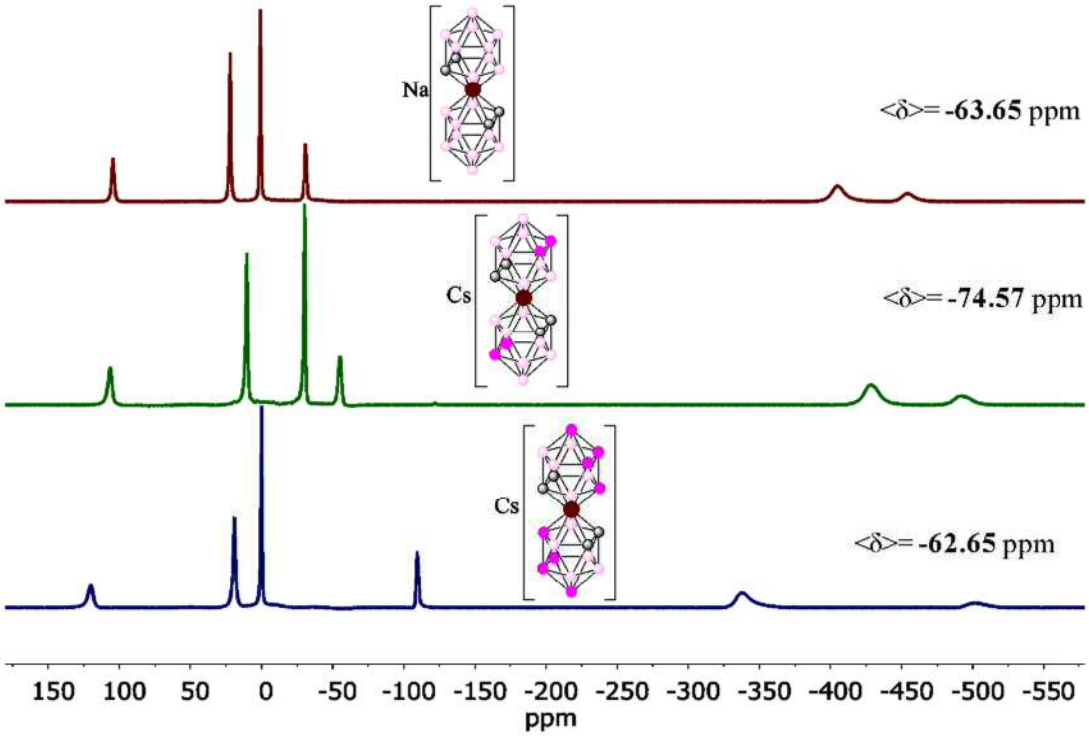

Figure 2.27. $^{11}B\{^1H\}$-NMR spectra of the Na[**4**] in red, Cs[I_4-**4**] in green and Cs[I_8-**4**] in blue.

moves 12 ppm to down field with respect to [I_4-**4**]$^-$ species.

Both species, paramagnetic Cs[I_8-**4**] and diamagnetic Cs_2[I_8-**4**], were characterized by IR, NMR and MALDI-TOF-MS spectroscopies. In addition, good crystals suitable for X-ray diffraction of Cs_2[I_8-**4**] were grown from a mixture solution of toluene : acetone.

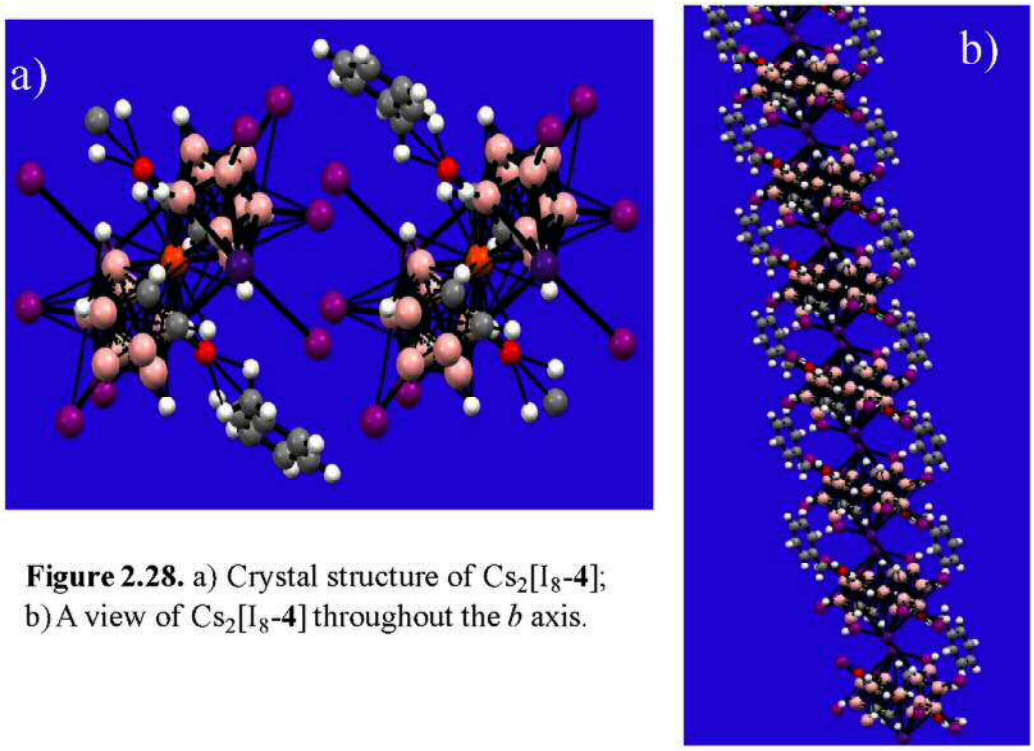

Figure 2.28. a) Crystal structure of Cs_2[I_8-**4**]; b) A view of Cs_2[I_8-**4**] throughout the *b* axis.

The crystal structure of Cs[3,3'-Fe(8,9,10,12-I_4-1,2-$C_2B_9H_7)_2]_2$, Cs_2[I_8-**4**], shows a two non-interacting 1D chains throughout the axis *a* that is shown in Figure 2.28a. The crystal structure through the axis *b* is shown in Figure 2.28b in which can be observed a 1D chain external wrapped through a molecule of H_2O to a toluene molecule. There are four iodine atoms bonded to each half C_2B_9 ligand moiety. Three of the four atoms are directly bonded to three Boron vertexes, B(9), B(12) and B(10) with B-I bonds distance of 3.519(9), 3.42(1) and 3.40(1), respectively. To be noticed that the B(8) vertex from the C_2B_3 pentagonal ligand face is bonded to a Cs atom that bridges in between the B(8) and I(8) forming B(8)-Cs-I(8). The B(8)-Cs and Cs-I(8) bonds distance are 2.240(9) and 3.932(1) Å

2.1.3.b.- Chlorinated derivatives

Once we have established the procedure that can be used in order to obtain the poly-chlorinated derivatives of cobaltabis(dicarbollide), the next step was to use it for the synthesis of chlorinated ferrabis(dicarbollide) clusters.

Several reactions by using 50 mg of Cs[**4**] with SO_2Cl_2 (1:1) in acetonitrile was achieved at 70°C in different period of time that goes in between 45 minutes and 140 hours as it is summarized in Table 2.7. As in the section 2.1.2.b, the mass spectroscopic technique MALDI-TOF-MS was the most suitable one to analyze chlorinated clusters of monoanionic [**4**]$^-$. The quantitative results of the chlorination reaction of ferrabis(dicarbollide) are very similar to the ones obtained with cobaltabis(dicarbollide) (see Table 2.7).

Entry	Time	[3,3'-Fe($C_2B_9H_{11-y}Cl_y$)($C_2B_9H_{11-z}Cl_z$)]						
		x = 5	x = 6	x = 7	x = 8	x = 9	x = 10	x = 11
1	86 h at room temperature	**18.86**	**64.52**	**16.61**				
2	45 min, 70^{0}C	**25.75**	**68.42**	**5.83**				
3	1 hour, 70^{0}C	**13.37**	**73.90**	**12.73**				
4	2 hours, 70^{0}C	**8.14**	**72.11**	**19.75**				
5	4 hours, 70^{0}C	**6.12**	**56.18**	**37.70**				
6	46 hours, 70^{0}C		**20.82**	**58.82**	**20.36**			
7	70 hours, 70^{0}C			**38.32**	**55.48**	**6.20**		
8	85 hours, 70^{0}C			**25.92**	**62.56**	**11.52**		
9	116 hours, 70^{0}C			**23.45**	**53.42**	**18.16**	**4.97**	
10	140 hours, 70^{0}C				**16.90**	**40.6**	**32.36**	**10.14**

Table 2.7. Percentage of the mixture of chlorinated derivatives of ferrabis(dicarbollide) as a function of time. x=y+z, x is the total number of chlorine atoms exchanged for hydrogen atoms in [NMe_4][**4**].

For the mixture pentasubstituted (13.37%), hexasubstituted (73.90%) and sevensubstituted (12.73%) that was obtained after 1 h heating, we tried to purify passing through a preparative layer chromatography, using ethyl acetate as eluent. Unfortunately, the separation of the 3 chlorinated compounds was not achieved. Another method for the synthesis of chlorinated derivatives of ferrabis(dicarbollide) was under pressure by using autoclave. In this procedure, [NMe_4][**4**], (166 mg, 0.42 mmol)

was solubilise with 1:1 mixture of SO_2Cl_2 and acetonitrile and place it in to the autoclave. After 2 h at 100-110°C and 1h at room temperature we obtained a dark green

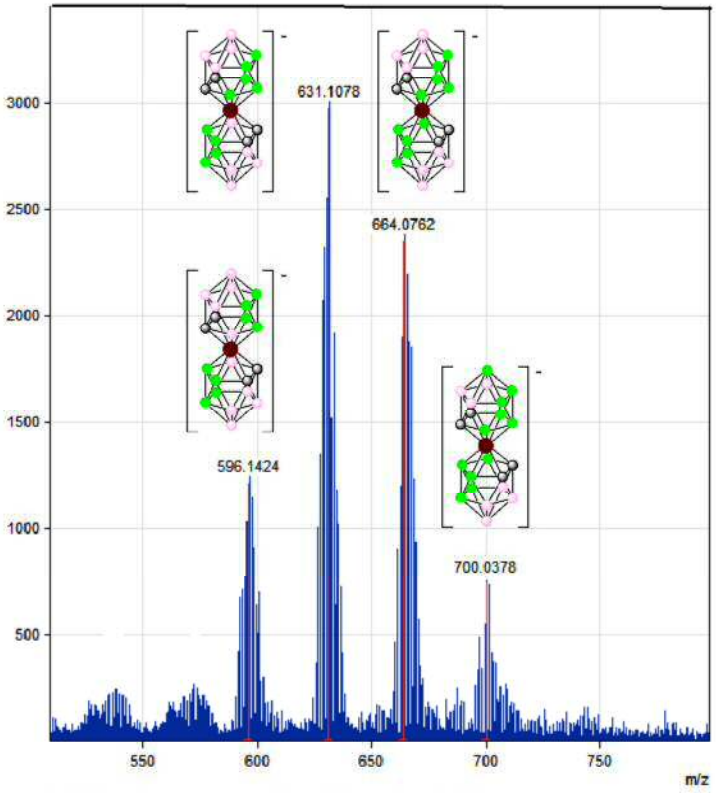

Figure 2.29. Negative MALDI-TOF-MS spectrum after 140 hours.

solution. The information that we extracted from the MALDI-TOF-MS spectrum, showed us a mixture of 3 compounds: heptasubstituted, $[Cl_7\text{-}\mathbf{4}]^-$ (15.70%), octasubstituted, $[Cl_8\text{-}\mathbf{4}]^-$ (64.88%) and ninesubstituted, $[Cl_9\text{-}\mathbf{4}]^-$ (19.42%) (Figure 2.30).

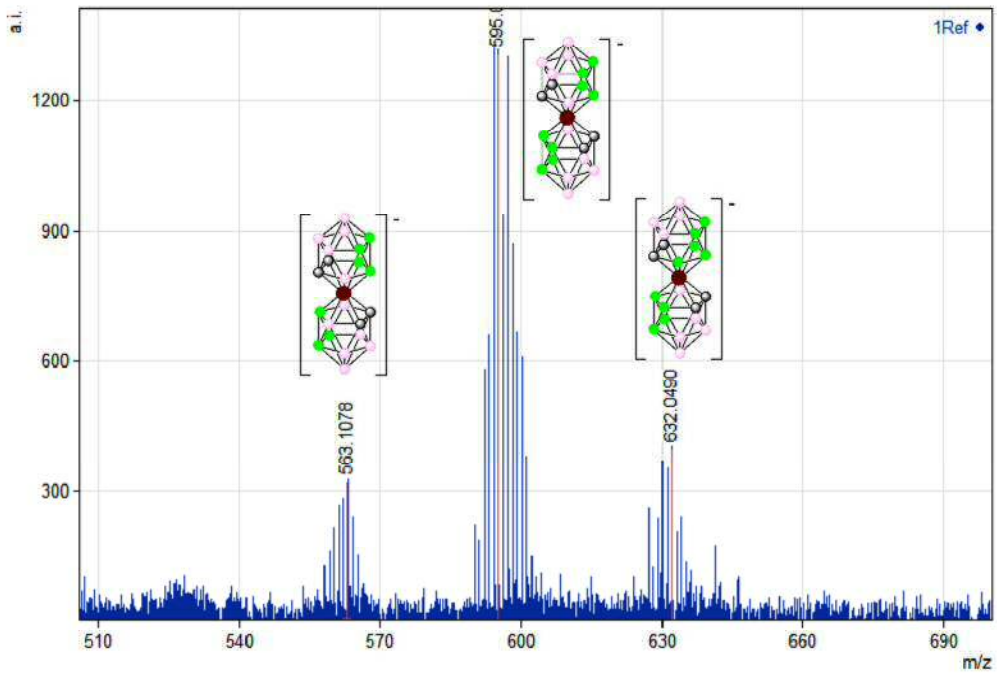

Figure 2.30. MALDI-TOF-MS spectrum after using the autoclave for 2 hours.

This method allows us to obtain in a very short time the octachlorinated derivative but also has some drawbacks. The reason why we did not carry on more experiments using the autoclave was because the mixture SO_2Cl_2 : acetonitrile is very corrosive (SO_2 and HCl are released from the reaction) and it can damage of the equipment.

After 72h of reflux at 70°C and the evaporation of the solvent, good crystals of $[NMe_4]_2[Cl_8$-**4**$]$ for X-ray diffraction, were obtained at room temperature from an acetone solution. The oxidation state of the metal and the number of chlorine atoms in the $[Cl_8$-**4**$]^{2-}$ molecule was fully confirmed.

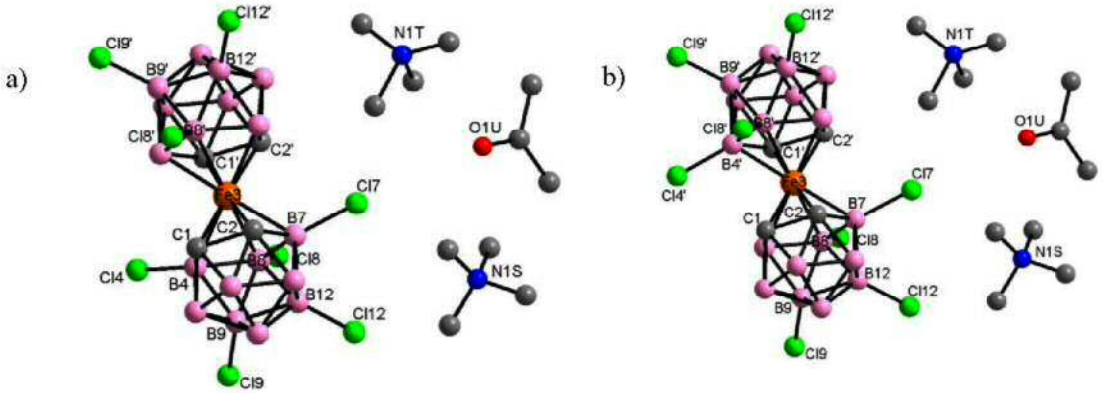

Figure 2.31. a) Crystal structure of $[NMe_4]_2[Cl_8$-**4**$]$ 40%; b) Crystal structure of $[NMe_4]_2[Cl_8$-**4**$]$ 60%.

3.1.- Study of different salts of parent [3,3'-Co(1,2-$C_2B_9H_{11}$)$_2$]$^-$ and of some of its derivatives: [Co(8-I-1,2-$C_2B_9H_{10}$)$_2$]$^-$, [Co(8-I-1,2-$C_2B_9H_{10}$)(1',2'-$C_2B_9H_{11}$)]$^-$ and [3,3'-Fe(1,2-$C_2B_9H_{11}$)$_2$]$^-$

Weakly Coordinating Anions (WCAs) are anionic ligands that have an extremely low tendency to bind to metal centers. They easily migrate from the metal center to yield an empty site to be occupied by a substrate, what makes them ideal for catalysis. [37] Recognized examples of WCAs are carboranes, boranes and metallacarboranes. These are deltahedra in which most or all of their vertexes are boron atoms.[37b,c] Very stable examples are the ones outlined in Figure 3.1: $[CB_{11}H_{12}]^-$, $[B_{12}H_{12}]^{2-}$ and [3,3'-Co(1,2-$C_2B_9H_{11}$)$_2$]$^-$, **[3]**$^-$. Their weak coordination tendency arises from their low charge density, [38] bulky size and sufficient charge delocalization. [39] However, over the past few years, several researchers have shown that some of the metallacarboranes are not as WCAs as it was thought and that did behave similarly to a surfactant in aqueous solutions. Wipff et al. interpreted by molecular dynamics methods that **[3]**$^-$ anions, although lacking the amphiphilic topology, behave as anionic surfactants.[28b] Later on, Matějíček et al. studied this anion in aqueous solution by a combination of static and dynamic light scattering and microscopy methods.[26] They observed that the compound organizes in spherical aggregates with a radii of around 100 nm in a fairly monodisperse way. More recently, Bauduin, Teixidor et al. demonstrated by small-, wide-angle X-ray and neutron scattering that H**[3]** forms monolayer vesicles at low concentrations in water which radii is approx 20 nm in the concentration range 1-13mM.[40] Increase in concentration leads to a phase transition from vesicles to small micelles and results in the coexistence of both aggregation states at higher concentrations. Finally, it has been proven that minor changes in the molecular structure of [3,3'-Co(1,2-$C_2B_9H_{11}$)$_2$]$^-$ induce major modifications in the solution behavior. The substitution of two B-H by two B-I in the

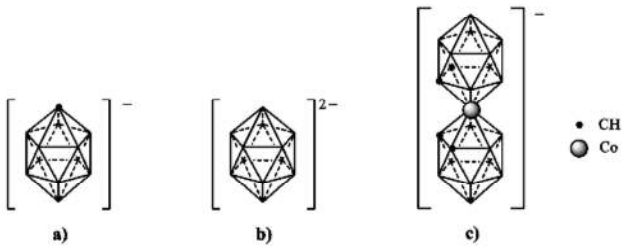

Figure 3.1. Schematic structure of some weakly coordinating anions (WCAs) based on boron clusters: (a) $[CB_{11}H_{12}]^-$, (b) $[B_{12}H_{12}]^{2-}$ and (c) **[3]**$^-$.

structure of [3,3'-Co(1,2-$C_2B_9H_{11}$)$_2$]$^-$ leads to a lamellae lyotropic phase in the high concentration regime.[41] This minor molecular alteration induces large self-organizing consequences that correlate very well with the concept of molecular materials. To progress in the understanding of the solution behavior of the metallacarboranes, the performance as electrolytes of [**3**]$^-$ and its chloroderivatives, [Cl_x-**3**]$^-$ (x=2-9), in the water electrolysis process was used to ascertain if under such conditions these compounds also manifest the surfactant properties. The experiments carried out, drawn on the grounds of I/V curves of water splitting into H_2 and O_2, fully support the sentence "although lacking the amphiphilic topology, metallacarboranes behave as anionic surfactants".[27] Surfactants are amphiphilic compounds meaning that they contain hydrophobic tails and hydrophilic heads. Metallacarboranes lack the amphiphilic topology characteristic of surfactants. However, metallacarboranes at low and high aqueous concentrations display many characteristics of surfactants. Despite both having a similar behavior, the type of forces that generate the aggregates are expected to be very different in the two cases. To get information on the interactions between adjacent parent [**3**]$^-$ clusters, we have searched the structures deposited in the Cambridge Structural Database (CSD).[42] In this way, [**3**]$^-$ has been found featuring a chain in which the metallacarborane clusters are bound one to the other through simple and double dihydrogen bonds B-H···H-C_c,[43] as outlined in Figure 3.2. Hence, the presence of both B-H and H-C_c bonds in the structure is likely to be responsible for the formation of intermolecular dihydrogen bonds that produce aggregates of [**3**]$^-$ in water.

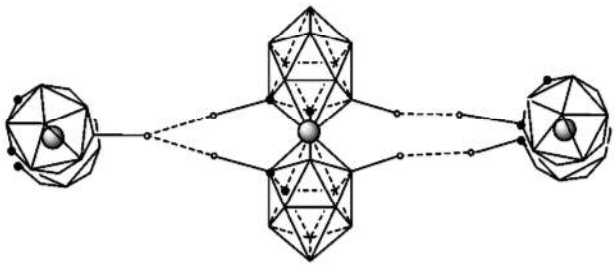

Figure 3.2. Molecular chain of [**3**]$^-$ stabilized by simple and double intermolecular dihydrogen bonds, shown here as dashed lines.

The B-H···H-C_c non-bonding interaction has been recently demonstrated.[41] Thus, the cluster C_c-H units in [**3**]$^-$ are ready to generate B-H···H-C_c dihydrogen bonds. When these assemblies are surrounded by water molecules, they adopt a stability conformation that avoids the direct contact of the connecting non-bonding interactions with water. Therefore, in an aqueous medium, [**3**]$^-$ tend to aggregate in supramolecular entities, and similarly to the surfactants, its periphery must face the water molecules. These interactions and the dimension of the aggregates prevents a facile rotation of the aggregate, thus of the

guests $[\mathbf{3}]^-$ molecules within the H_2O frame; the consequence is a widening of the ^1H-NMR resonances in water. Further evidence of the distinct behavior of formation of $[\mathbf{3}]^-$ aggregates in water was encountered in the ^{11}B- and $^{11}B\{^1H\}$-NMR in aqueous solution.[27] The ^{11}B-NMR of H[**3**] exhibits much wider signals in water than in an organic solvent that would cause the destruction of the aggregates and, consequently, the existence of free monomers. Figure 3.3 compares the ^{11}B-NMR spectrum a 0.1 M solution of H[**3**] in water (—) and in diethyl ether (···).

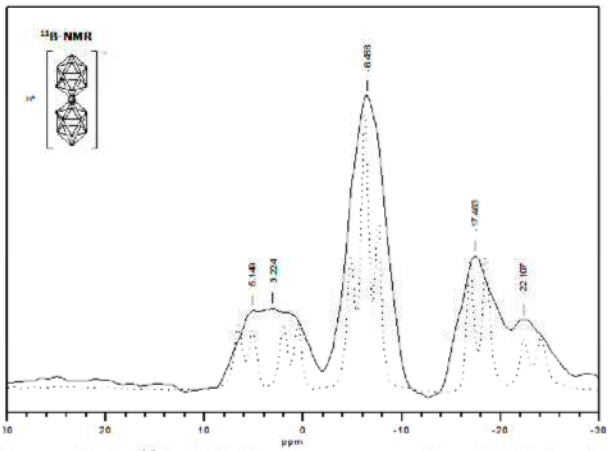

Figure 3.3. ^{11}B-NMR spectrum of a 0.1 M solution of H[**3**] in water (—) and in diethyl ether ( ).

3.1.1. NMR study of the H^+, Li^+, Na^+ and K^+ salts of $[3]^-$

The acid salt of cobaltabis(dicarbollide) H[**3**] was proven to form monolayer vesicles about 50 nm in diameter at concentration smaller than 13 mM in water. However, a large increase in the hydrodynamic diameter from 50 to 890 nm is observed after the addition of NaCl. The hollow structure of the vesicles was observed by Cryo-TEM (Figure 3.4). Increasing concentration leads to a Coulomb explosion of the closely packed monolayer vesicles into small micelles (Figure 3.5). This results is the coexistence of both aggregation states at higher

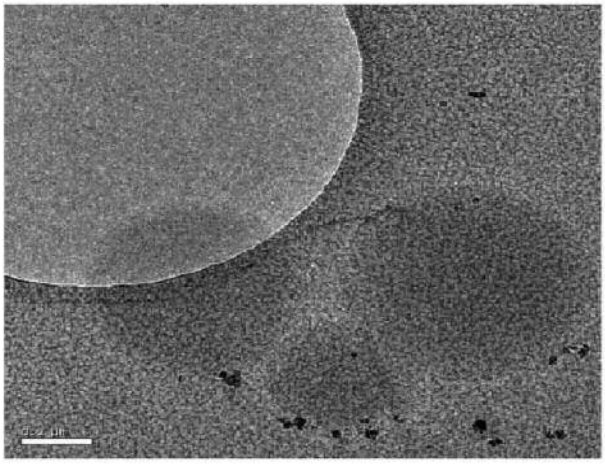

Figure 3.4. Visualization of vesicles structure by Cryo-TEM.

concentration than 13 mM. The formation of monolayer vesicles and small micelles was so far unknown for water soluble carborane derivatives.[40]

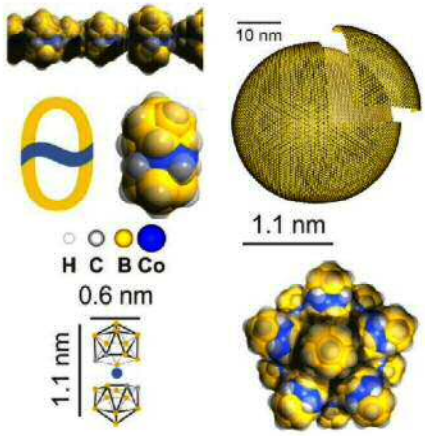

Figure 3.5. The cobaltabisdicarbollide anion, $[\mathbf{3}]^-$ is composed of two bulky and hydrophobic dicarbollide semicages (yellow) that "sandwich" a cobalt(III) ion as the polar part (blue). Hydrogen atoms are omitted for clarity in the crystal structure.

Following these studies, the Na^+, K^+ and Li^+ salts of cobaltabis(dicarbollide) were prepared by cation exchange: this procedure was done for the first time in this thesis as an advanced alternative to the extraction procedure in diethyl ether that leads primarily to the protonated cobaltabis(dicarbollide).[44] To get the desired cation counterbalancing the cobaltabis(dicarbollide), appropriately 100 mg of starting Cs[**3**] compound was dissolved in a minimum volume of acetonitrile/water (50:50). Then, the solution of Cs[**3**], and was passed repeatedly through a cation exchanging resin, previously loaded with the desired cation. The solvent mixture was finally evaporated. The partial or complete solubilization of the new salt in distilled water was indicative of the full cation exchange or, alternatively if $[NMe_4]$[**3**] was the starting material, the disappearance of the $[NMe_4]^+$ peak in the ^{1}H-NMR was diagnostic of complete exchange to the desired alkaline ion. Salts of H^+, Li^+, Na^+ and K^+ of $[\mathbf{3}]^-$ were obtained by this procedure.

NMR measurements give information on the molecules in the bulk of the solution, therefore providing information on their aggregation in one particular solvent. To further evidence the distinct behavior of the anions $[\mathbf{3}]^-$, $[\text{I-}\mathbf{3}]^-$, $[\text{I}_2\text{-}\mathbf{3}]^-$, the ^{11}B{^{1}H} and ^{1}H{^{11}B}-NMR studies in D_2O of the H[**3**], Li[**3**], Na[**3**], K[**3**], H[I-**3**], Na[I-**3**], H[I_2-**3**] and Na[I_2-**3**] at different concentrations: 2.5, 5, 10, 20, 30, and 60 mM were carried out.

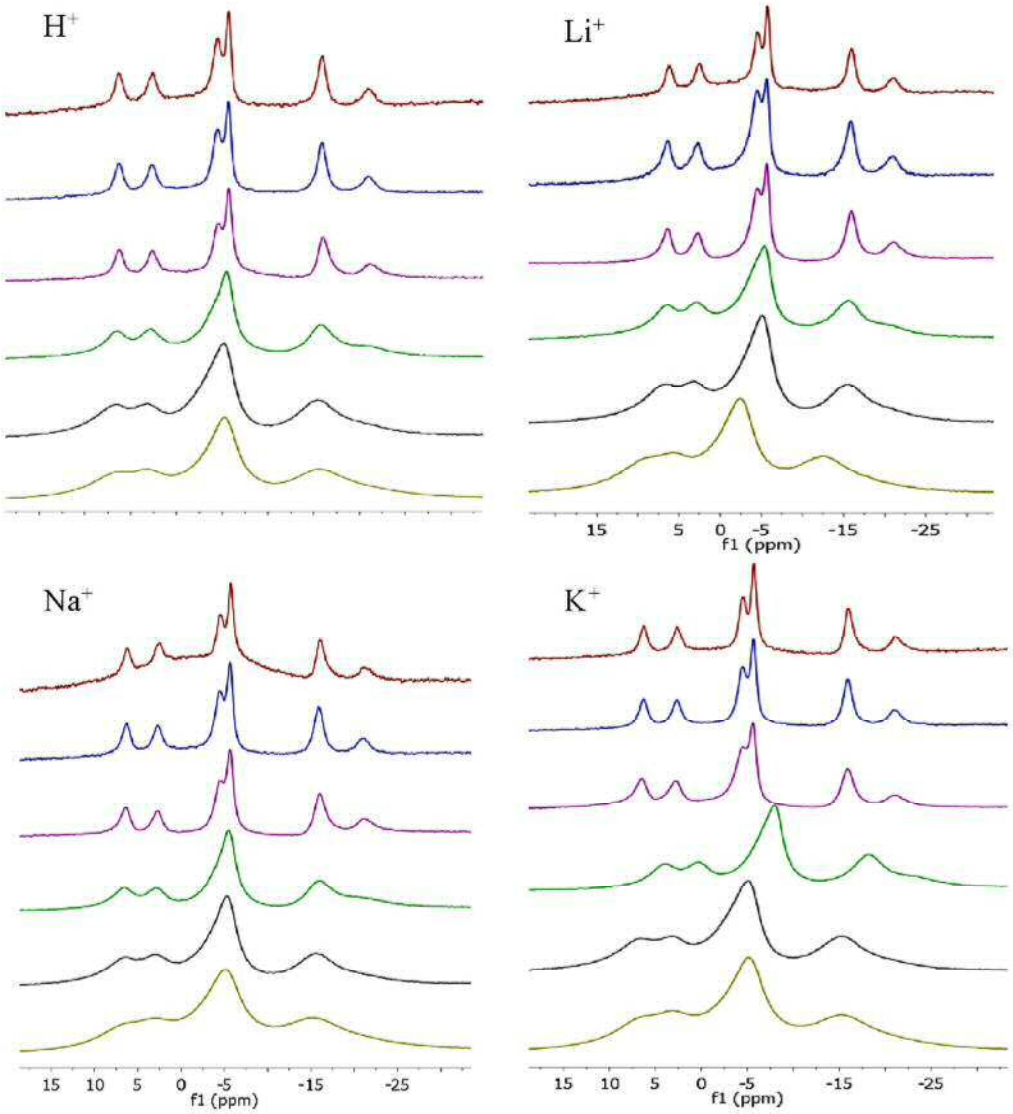

Figure 3.6. $^{11}B\{^1H\}$ studies in D_2O of the H[**3**], Li[**3**], Na[**3**], K[**3**] at different concentrations: 2.5 (in red), 5 (in blue), 10 (in purple), 20 (in red), 30 (in black) and 60 mM (in light green).

It is easily observed from the $^{11}B\{^1H\}$-NMR spectra of Li[**3**], Na[**3**] and K[**3**] that wider resonances are found at concentrations higher than 10 mM indicating the presence of micelles, as reported by H[**3**] that is taken as a reference. It also corresponds with the lost of sharpness the almost lost of the peak near -21 ppm.

The $^1H\{^{11}B\}$-NMR spectra of H[**3**], Li[**3**], Na[**3**] and K[**3**] (Figure 3.7), indicate that the resonance of the C_c-H remains invariant in the concentration range 2.5 - 10 mM in which, the vesicles are formed. However, when the concentration increases till 20 mM at which concentration the micelles are formed, the C_c-H resonance is shifted upfield for all salts. This is consistent with a phase transformation of the cobaltabis(dicarbollide) in which the vesicular C_c-H···H-B dihydrogen bonds are altered

into the micellar C_c-H···H-B dihydrogen bonds. The influence of this weak interaction on the B-H resonances was not seen.

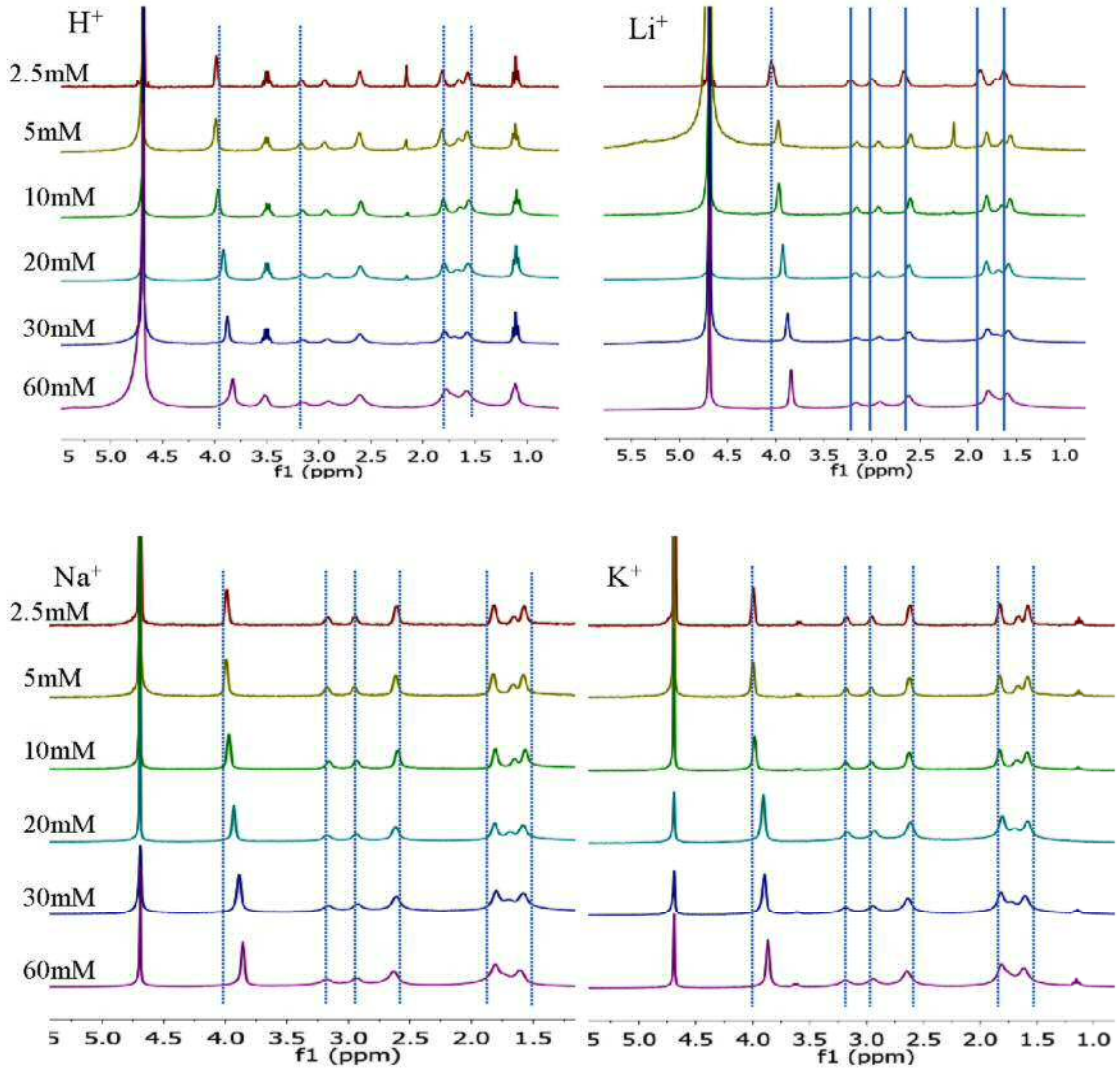

Figure 3.7. ^{1}H $\{^{11}B\}$ studies in D_2O of the H[**3**], Li[**3**], Na[**3**], K[**3**] at different concentrations: 2.5 (in red), 5 (in light green), 10 (in green), 20 (in light blue), 30 (in blue) and 60 mM (in purple).

The IR spectrum of the H[**3**] / Li[**3**] / Na[**3**] salts of the anion [**3**]$^-$ clearly show two different stretching frequencies of the C_c-H bond and in addition, all salts display frequencies at 3591-3513 and 1641-1506 cm^{-1} that are related to the presence of coordinated water.

Table 3.1 displays the IR, ^{1}H- and ^{1}H $\{^{11}B\}$-NMR spectroscopies of compounds H[**3**], Li[**3**], Na[**3**], K[**3**] and Cs[**3**] that acts as a reference. The Na[**4**] is included to compare with Na[**3**].

Compound	υ (C_c-H)	υ (B-H)	υ (O-H)	δ (C_c-H)	δ (B-H)
H[**3**]	3047 3026	2575 / 2557 2513	3581 / 3508 3456 1648 / 1506	3.97	3.16, 2.93, 2.60, 1.81, 1.65, 1.56
Li[**3**]	3045 3031	2619 / 2596 2575 / 2518	3640 / 3586 3513 1641 / 1610	3.97	3.16, 2.94, 2.60, 1.81, 1.66, 1.57
Na[**3**]	3047 3029	2614 / 2581 2544 / 2521	3591 / 3560 3515 1638 / 1605	3.97	3.16, 2.93, 2.60, 1.81, 1.65, 1.56
K[**3**]	3042	2570 / 2537 2513	3593 / 3523 1605	3.98	3.18, 2.95, 2.62, 1.83, 1.68, 1.59
Cs[**3**]	3042	2610 / 2574 2538 / 2510	-	3.96	3.40, 2.99, 2.72, 1.95, 1.64, 1.59
Na[**4**]	3037 3021	2565 / 2521	3590 / 3562 3521 1635 / 1605	41.09	68.65, -0.30, -3.16, -11.88
Na[I_2-**3**]	3042	2628 / 2589 2560 / 2529	3555 / 3446 1597	4.55	3.08, 2.99, 2.49, 2.12, 1.84

Table 3.1. IR, ^{1}H- and ^{1}H{^{11}B}-NMR spectroscopies of compounds H[**3**], Li[**3**], Na[**3**], K[**3**], Cs[**3**], Na[**4**] and Na[I_2-**3**].